Multi-decadal fluctuations in root zone storage capacity through vegetation adaptation to hydro-climatic variability has minor effects on the hydrological response in the Neckar basin, Germany.

Siyuan Wang[1], Markus Hrachowitz[1], Gerrit Schoups[1]

[1]Department of Water Management, Faculty of Civil Engineering and Geosciences, Delft University of Technology, Stevinweg 1, 2628CN Delft, Netherlands

Correspondence to: Siyuan Wang (S.Wang-9@tudelft.nl)

Abstract. Climatic variability can considerably affect the catchment-scale root zone storage capacity (S_{umax}) which is a critical factor regulating latent heat fluxes and thus the moisture exchange between land and atmosphere as well as the hydrological response and biogeochemical processes in terrestrial hydrological systems. However, direct quantification of changes in S_{umax} over long time periods and the mechanistic drivers thereof at the catchment-scale are missing so far. As a consequence, it remains unclear how climatic variability, such as precipitation regime or canopy water demand, affects S_{umax} and how fluctuations in S_{umax} may influence the partitioning of water fluxes and therefore, also affect the hydrological response at the catchment-scale. Based on long-term daily hydrological records (1953-2022) in the Upper Neckar river basin in Germany, we found that variability in hydroclimatic conditions, with aridity index I_A (i.e. E_P/P) ranging between ~ 0.9 and 1.1 over multiple consecutive 20-year periods was accompanied by deviations ΔI_E between -0.02 and 0.01 from the expected I_E inferred from the long-term parametric Budyko curve. Similarly, fluctuations in S_{umax}, ranging between ~95 and 115 mm or ~20%, were observed over the same time period. While uncorrelated with long-term mean precipitation and potential evaporation, it was shown that the magnitude of S_{umax} is controlled by the ratio of winter over summer precipitation ($p < 0.05$). In other words, S_{umax} in the study region does not depend on the overall wetness condition as for example expressed by I_A, but rather on how water supply by precipitation is distributed over the year. However, fluctuations in S_{umax} were found to be uncorrelated with observed changes in ΔI_E. Consequently, replacing a long-term average, time-invariant estimate of S_{umax} with a time-variable, dynamically changing formulation of that parameter in a hydrological model did not result in an improved representation of the long-term partitioning of water fluxes, as expressed by I_E (and fluctuations ΔI_E thereof), nor in an improved representation of the shorter-term response dynamics.

Overall, this study provides quantitative mechanistic evidence that S_{umax} significantly changes over multiple decades reflecting vegetation adaptation to climatic variability. However, this temporal evolution of S_{umax} cannot explain long-term fluctuations in the partitioning of water (and thus latent heat) fluxes as expressed by deviations ΔI_E from the parametric Budyko curve over multiple time periods with different climatic conditions. Similarly, it does not have any significant effects on shorter term hydrological response characteristics of the upper Neckar catchment. This further suggests that accounting for temporal evolution of S_{umax} with a time-variable formulation of that parameter in a hydrological model does not improve its ability to

reproduce the hydrological response and may therefore be of minor importance to predict the effects of a changing climate on the hydrological response in the study region over the next decades to come.

1 Introduction

Vegetation is a key component of the terrestrial hydrological cycle as it shapes the hydrological functioning of catchments by regulating the long-term average partitioning of water into drainage and evaporative fluxes (i.e. latent heat), frequently expressed as runoff ratio $C_r = Q/P$ [-] and evaporative index $I_E = 1 - Q/P = E_A/P$ [-], respectively. More specifically, vegetation transpiration, that in spite of uncertainties (Coenders-Gerrits et al., 2014) globally constitutes the largest fraction of all evaporative fluxes (Jasechko, 2018), is systematically controlled by the interplay between canopy water demand and water supply from the subsurface (Donohue et al., 2007; Yang et al., 2016b; Jaramillo et al., 2018a; Mianabadi et al., 2019). To survive, vegetation needs continuous access to water stored in the subsurface and accessible to roots to satisfy its canopy water demand. As a consequence, the vegetation present at any moment, and in particular its active root system, reflects its successful adaptation to the prevalent climatic conditions in a region (Laio et al., 2001; Schenk and Jackson, 2002; Rodriguez-Iturbe et al., 2007; Donohue et al., 2007; Gentine et al., 2012; Liancourt et al., 2012). Irrespective of geometry, distribution or structure of root systems, the *maximum* vegetation-accessible water storage volume in the unsaturated root zone of the subsurface, hereafter referred to as root zone storage capacity S_{umax} [mm], represents the hydrologically relevant information of root systems (Rodriguez-Iturbe et al., 2007; Nijzink et al., 2016a; Savenije and Hrachowitz, 2017; Gao et al., 2024). Therefore, the S_{umax} is directly reflects the hydrologically relevant information of root-systems at the catchment-scales. In response to a changing environment, these root systems of vegetation continuously adapt to allow the most efficient use of available energy and resources for surviving. The driving factors of changes in root systems are thus also the driving factors for changes in S_{umax}, as S_{umax} inherently represents adaptations of the root system.

As a central part of hydrological systems, S_{umax} is also a critical parameter in hydrological and land-surface models. As such, it can, in principle, be estimated as a function of root depths and the subsurface pore volume between field capacity and permanent wilting point (Scrivner and Ruppert, 1970; Sivandran and Bras, 2012, 2013). However, these data are typically not available at sufficient levels of detail. Alternatively, catchment-scale S_{umax} can be estimated by three broad approaches. Firstly, it can be obtained by calibration as parameter of a hydrological model (Nijzink et al., 2018; Bouaziz et al., 2020; Wang et al., 2023; Sriwongsitanon et al., 2023; Roberts et al., 2021; Bahremand and Hosseinalizadeh, 2022; Sadayappan et al., 2023; Tong et al., 2022). Secondly, based on optimality principles, there are some variables like transpiration, nitrogen uptake or carbon gain that can be maximized to quantify S_{umax} (Guswa, 2008; McMurtrie et al., 2012; Sivandran and Bras, 2012; Yang, et al., 2016b; Speich et al., 2018). Thirdly, S_{umax} can be robustly estimated at the catchment scale directly from annual water deficits based on observed hydro-climatic data, i.e. precipitation and transpiration (e.g., Donohue et al., 2012; Gentine et al., 2012; Gao et al., 2014b; De Boer-Euser et al., 2016; Nijzink et al., 2016a; Dralle et al., 2021; McCormick et al., 2021; Hrachowitz et al., 2021; Stocker et al., 2023; van Oorschot et al., 2021, 2024). For applications of hydrological and land-surface models

S_{umax} (or equivalent parameters) has, except for very few exceptions (Wagener et al., 2003; Merz et al., 2011; Bouaziz et al. 2022; Tempel et al., 2024) been assumed constant over time. As a major knowledge gap, it remains so far unknown if S_{umax} follows climatic variability and evolves over time, thereby reflecting vegetation adaptation to changing conditions.

In contrast, it is well understood that, due to the importance of vegetation for the hydrological functioning of terrestrial systems, anthropogenic land use management practices, such as de- and afforestation (Brown et al., 2005; Brath et al., 2006; Fenicia et al., 2009; Alila et al., 2009; Jaramillo et al., 2018a; Teuling et al., 2019; Stephens et al., 2021; Hoek van Dijke et al., 2022; Ellison et al., 2024) or irrigation (e.g. AghaKouchak et al., 2015; Van Loon et al., 2016; Roodari et al., 2021) can induce major shifts in the partitioning between the major components of the terrestrial water and energy cycles, and thus between I_E and C_r. Two detailed recent studies with well documented information on deforestation in several experimental catchments could establish explicit mechanistic links between the reduction of S_{umax} by > 50% following deforestation and decreases in I_E (and thus increases in C_r) from ~ 0.4 – 0.5 to ~ 0.1 – 0.3, depending on the catchment and the scale of deforestation (Nijzink et al.,2016a; Hrachowitz et al., 2021).

Mapping the shifts to lower I_E that followed these land conversions from forest to grass- and rangeland type vegetation as a function of the aridity index $I_A = E_P/P$ in the Budyko framework (Schreiber, 1904; Ol'Dekop, 1911; Budyko, 1974) corresponds well to the results of previous studies that suggest that, across the world, catchments dominated by grass exhibit consistently lower I_E at the same I_A than forest environments (e.g. Zhang et al., 2001, 2004; Oudin et al., 2008). These differences in long-term average I_E are accounted for by parametric reformulations of the Budyko framework, such as the Tixeront-Fu equation (Tixeront, 1964; Fu, 1981). The lumped parameters (here: ω) of these expressions define long-term average catchment-specific positions in the $I_A – I_E$ space. As such, the parameters are typically interpreted to encapsulate vegetation characteristics and all other hydro-climatic and physiographic properties of individual catchments besides I_A (e.g. Roderick and Farquhar, 2011; Berghuijs and Woods, 2016). A frequent assumption is that with changes in climatic conditions, here represented by I_A, individual catchments can be expected to move to the associated new positions I_E, following their specific trajectories defined by ω (e.g. Zhou et al., 2015; Bouaziz et al., 2022). However, several studies have demonstrated that catchments in many regions world-wide experience deviations ΔI_E from their expected new I_E following a change in I_A (e.g. Jaramillo and Destouni 2014; van der Velde et al., 2014; Jaramillo et al., 2018a; Reaver et al., 2022; Ibrahim et al., 2024; Tempel et al., 2024).

From the above the following questions arise: (1) following the notion that vegetation, i.e. individual plants but also the species composition of plant communities, continuously adapts to climatic conditions, does catchment-scale root zone storage capacity S_{umax} change over multi-decadal time scales? (2) do multi-decadal changes in the vegetation response, expressed by changes in S_{umax}, explain deviations ΔI_E from expected I_E? (3) does a time-variable representation of S_{umax} as parameter in a hydrological model improve the models' ability to reproduce the hydrological response?

Building on previous studies, the objectives of this study in the Upper Neckar river basin in Germany are therefore to provide an analysis of multi-decadal changes in S_{umax} as a result of changing climatic conditions over a 70-year period (1953 – 2022) and how this further affects hydrological dynamics. More specifically, we test the hypotheses that (1) S_{umax} significantly changes over multiple decades reflecting vegetation adaptation to climatic variability, (2) changes in S_{umax} affect the long-term

partitioning of drainage and evaporation and thus control deviations ΔI_E from the catchment-specific trajectory in the Budyko space and (3) a time-dynamic implementation of S_{umax} improves the representation of streamflow in a hydrological model.

2 Study area

The Upper Neckar River basin in South-West Germany covers an area of ~4000 km^2, with the Black Forest on the western part and the Swabian Jura on the southeastern side. The river basin has a varying topography with the elevation ranging from 250 m at the outlet in the north to about 1019 m in the South (Fig. 1a; Table 1). Following the elevation gradient, the landscape is dominated by terrace-like elements and undulating hills (~50%) with wide valleys used as grass- and croplands in lower regions, in particular in the southeastern parts of the Upper Neckar Basin, and increasingly steep and narrow forested valleys (~40%) towards the southern parts and the remaining area including flat grassland in valley bottoms (~10%) (Fig. 1c). Annual mean precipitation (P) over the whole river basin has a considerable spatial heterogeneity ranging from ~700 mm yr^{-1} in the lower parts of the basin to ~1600 mm yr^{-1} over the Black Forest with catchment average long-term mean precipitation (P) reaching ~880 mm yr^{-1} (Fig. 1b, Table 2). The catchment is characterized by a temperate-humid climate, with warm, wet summers and cold, drier winters. Precipitation exhibits some seasonality with ~500 mm yr^{-1} for summer months (from May to October) and ~380 mm yr^{-1} for winter months (from November to April), respectively (Fig 3). Although snow is in general not a major component of precipitation in the study region, snowmelt can have a significant influence during individual storm events. The long-term mean temperature is about 8.2 °C and potential evaporation (E_P) is around ~860 mm yr^{-1} with an aridity index $I_A = E_P/P$ ~0.97 (Table 2).

3 Data sets

3.1 Data

Daily hydro-meteorological data were available for the period 01/01/1953 – 31/12/2022 (Fig. 2). Daily precipitation and daily mean air temperature were obtained from stations operated by the German Weather Service (DWD). Precipitation was recorded at 15 stations and temperature measurements were available at 8 stations (Fig. 1) in or close to the study basin. Daily potential evaporation E_P (mm d^{-1}) was estimated using the Hargreaves equation based on the observed daily maximum and minimum temperature, which has been used in many previous studies and shown to be a suitable method for modelling applications (Oudin et al., 2005). Daily mean discharge data for the period 01/01/1953 – 31/12/2022 at the outlet of the upper Neckar basin at Plochingen station were provided by the German Federal Institute of Hydrology (BfG). In addition, data of daily mean discharge for the same time period from three sub-catchments within the upper Neckar basin (Fig.1) at the gauges Rottweil (C1; 422 km^2), Plochingen at Fils river (C2; 706 km^2) and Horb (C3; 1111 km^2) were available from the Environmental Agency of the Baden-Württemberg region (LUBW).

Based on the CORINE Land Cover data set of the upper Neckar river basin during the period 01/01/1953 – 31/12/2022

(https://land.copernicus.eu/pan-european/corine-land-cover), there is only very minor change (< 2%) for all defined land cover classes (Fig. 1c). The 90 m × 90 m digital elevation model of the study region (Fig. 1a) was obtained from the HDMA database of the USGS (Verdin, 2017; https://doi.org/10.5066/F7S180ZP) and used to derive the local topographic indices including height above nearest drainage (HAND) and slope.

3.2 Data pre-processing

For the subsequent experiment (section 4.2), the study basin was stratified into three zones P1 – P3 that are characterized by distinct long-term precipitation pattern (hereafter: precipitation zones), following the approach described and implemented for the Neckar basin by Wang et al. (2023). Briefly, Goovaerts (2000) and Lloyd (2005) showed that areal precipitation estimates informed by elevation data were often more accurate than those based on precipitation gauge observations alone (e.g. Hrachowitz and Weiler, 2011). Thus, to interpolate and to estimate areal precipitation across the basin we used Co-Kriging, considering elevation, as a preliminary analysis suggested lower errors. Finally, the individual precipitation estimates for each grid cell were used with K-means clustering to establish three clusters, representing the three precipitation zones P1 – P3 (see Fig. 1b).

To explore the fluctuations of S_{umax} over long time scales, we independently estimate root zone storage capacity S_{umax} for four subsequent sub-periods of the available data record ($t_1 - t_4$ in Table 2). To be survive, root systems of vegetation and the associated vegetation-accessible water storage capacity S_{umax} respond to the ever-changing conditions of its environment. However, as these changes occur at landscape scale and are mostly reflected by changes in the composition of plant species present in a specific spatial domain, fluctuations in S_{umax} occur largely at time-scales that reflect the life-cycles of individual plants. Thus, periods of at least 20-years are required to reflect this and to allow for meaningful estimates of S_{umax}, as also demonstrated by many other studies (e.g. Gao et al., 2014; Wang-Erlandsson et al., 2016; Singh et al., 2020; Stocker et al., 2023). We therefore had to strike a balance between the number of independent time periods (here: $t_1 - t_4$) and the robustness of the associated S_{umax} estimates. We deliberately chose to emphasize fewer but longer time periods and thus rather reliable estimates of S_{umax}.

4 Methods

To test the hypotheses that the key vegetation parameter, i.e. the root zone storage capacity S_{umax}, evolves over multi-decadal timescales in response to changing hydro-climatic conditions and controls the deviations from expected trajectories in the Budyko space, thereby reflecting the need for time-variable implementations of S_{umax} as parameter in a hydrological model, the following stepwise approach is designed: (1) Estimate the *observed* deviations ΔI_E from the long-term average expected I_E for four consecutive periods $t_1 - t_4$ in the study period (Table 2), (2) Estimate the root zone storage capacity over the entire study period ($S_{umax,WBT}$) as well as for the four individual periods $t_1 - t_4$ ($S_{umax,WBt}$) based on *observed* water balance data, (3) Estimate the root zone storage capacity over the entire study period ($S_{umax,calT}$) and the four individual periods $t_1 - t_4$ ($S_{umax,cal,t}$)

by *calibration* of a hydrological model over the respective time periods to evaluate whether the changes in calibrated $S_{umax,cal}$ reflect changes in $S_{umax,WB}$ directly estimated from water balance data from step (2), (4) Estimate the *modelled* deviations ($\Delta I_{E,mT,O'}$) from expected I_E using both, a long-term average time-invariant $S_{umax,WBT}$ and individual $S_{umax,WBt}$ for the four periods $t_1 - t_4$ as model parameters.

4.1 Estimation of the temporal trajectory in the Budyko framework

Mapping aridity $I_A = E_P/P$, where E_P is potential evaporation [mm d^{-1}] and P is precipitation [mm d^{-1}], against the evaporative index $I_E = E_A/P = 1 - Q/P$, where E_A is actual evaporation [mm d^{-1}] and Q is stream flow [mm d^{-1}], the Budyko framework is an expression of the long-term average water balance for a catchment. It is based on the assumption of negligible storage change over the averaging time period, i.e. $dS/dt \sim 0$. As demonstrated by Han et al. (2020), this assumption holds for averaging periods ≥ 10 years for a large majority of catchments worldwide. Note, that hereafter the term evaporation is used to refer to all combined evaporative fluxes, including interception and soil evaporation (E_i) as well as transpiration (E_T), following the terminology proposed by Savenije (2004) and Miralles et al. (2020).

The analysis in this paper is based on the parametric Tixeront-Fu formulation of the Budyko framework (Tixeront, 1964; Fu, 1981):

$$I_{E,T} = 1 + I_{A,T} - (1 + I_{A,T}^{\omega_T})^{1-\omega_T} \tag{1}$$

where $I_{E,T}$ is the observed evaporative index based over a chosen averaging period T, $I_{A,T}$ is the observed aridity index over the same period and ω_T is the associated catchment-specific parameter that represents all combined catchment properties other than I_A.

In a theoretical catchment that only experiences changes in I_A and no changes in any other hydro-climatic and/or physical catchment characteristics, it can be assumed that ω_T remains constant over time so that $\omega_T = \omega_{t_i} = \omega_{t_{i+1}}$. This implies that following a disturbance ΔI_A in a subsequent time period t_{i+1} the catchment stays on its specific curve defined by ω_T, to a new $I_{Et_{i+1}}$. In such a case, ω_T can thus be used to predict future hydrological partitioning I_E. Based on this assumption, we here use the complete available hydro-climatic data record to estimate the long-term average ω_{OT} as reference over the entire 1953 – 2022 study period. The sub-division into the four time periods $t_1 - t_4$ as shown in Table 2, then allowed to estimate the expected $I_{E,t_i'}$ in the individual periods $t_1 - t_4$: depending on the shift in the observed aridity index along the x-axis in t_i ($\Delta I_{A,T,ti} = I_{A,t_i} - I_{A,T}$), a catchment will move along its parametric Budyko curve defined by ω_{OT} to a new expected position $I_{E,t_i'}$ (Fig. 4).

Based on the available data we then estimate the individual observed I_{E,t_i} together with the associated ω_{t_i} for each of the four time periods $t_1 - t_4$ (Fig. 5) For each of the four time periods $t_1 - t_4$ the deviation of I_{E,t_i} from the catchment-specific expected $I_{E,t_i'}$, corresponding to a shift from ω_T to $\omega_{t_i} \neq \omega_T$ was then computed as $\Delta I_{E,t_i,t_i'} = I_{E,t_i} - I_{E,t_i'}$.

4.2 Estimation of root zone storage capacity derived by water balance method S$_{umax,WB}$

190 The root zone storage capacity is the *maximum* volume of water which can be held in soil pores of the unsaturated zone and which is accessible to root systems of vegetation for transpiration. Here the water balance method that is in detail described in previous papers (e.g. Gao et al., 2014b; Nijzink et al., 2016a; de Boer-Euser et al., 2016; Wang-Erlandsson et al., 2016; Bouaziz et al., 2020; Hrachowitz et al., 2021) is used to determine S$_{umax,WB}$. Briefly, S$_{umax,WB}$ is estimated based on daily observations of precipitation (P), potential evaporation (E$_P$) and stream flow (Q). As a first step, effective precipitation P$_e$ [mm d^{-1}] that

195 enters the subsurface is computed by accounting for interception evaporation by:

$$P_e(t) = P(t) - E_i(t) - dS_i/dt \tag{2}$$

where E$_i$ (mm d^{-1}) is daily interception evaporation, S$_i$ (mm) is the interception storage. For each time step, E$_i$ is determined by:

200
$$E_i(t) = \begin{cases} E_P(t) & if \ E_P dt < S_i \\ \frac{S_i}{dt} & if \ E_P dt \geq S_i \end{cases} \tag{3}$$

Then further to estimate the effective precipitation P$_e$ (mm d^{-1}) according to:

$$P_e(t) = \begin{cases} 0 & if \ S_i < S_{imax} \\ \frac{S_i - S_{imax}}{dt} & if \ S_i \geq S_{imax} \end{cases} \tag{4}$$

where S$_{imax}$ (mm) is the maximum interception storage. As S$_{umax}$ is not very sensitive to the choice of S$_{imax}$ as previously shown

205 by Hrachowitz et al., (2021) and Bouaziz et al. (2022), we used here a value of S$_{imax}$ = 2 mm, which was previously also used by de Boer-Euser et al. (2016).

Hereafter, the long-term mean transpiration $\overline{E_r}$ (mm d^{-1}) is estimated from the long-term water balance, with the assumption of no additional gains or losses:

$$\overline{E_r} = \overline{P_e} - \overline{Q_O} \tag{5}$$

210 where $\overline{P_e}$ (mm d^{-1}) is the long-term mean effective precipitation and $\overline{Q_O}$ (mm d^{-1}) is the long-term mean observed streamflow. Considering the seasonal fluctuation of energy input, the daily transpiration E$_r$ (mm d^{-1}) is estimated by subsequently scaling the daily potential evaporation E$_P$ (mm d^{-1}) minus the interception evaporation E$_i$ (mm d^{-1}) (see Eqs.2, 3) by the long-term mean transpiration $\overline{E_r}$ (mm d^{-1}), according to (Bouaziz et al., 2022, Hrachowitz et al., 2021):

$$E_r(t) = \frac{\overline{E_r}}{(\overline{E_P} - \overline{E_i})} (E_P - E_i) \tag{6}$$

215 Where $\overline{E_P}$ (mm d^{-1}) is the long-term mean potential evaporation, $\overline{E_i}$ (mm d^{-1}) is the long-term mean interception evaporation. From daily storage deficits S$_{rd,n}$ (t) (mm) during dry periods, estimated as the cumulative sum of daily effective precipitation P$_e$ (mm d^{-1}) minus transpiration E$_r$ (mm d^{-1}), the maximum storage deficit S$_{rd,n}$ of a specific year n is then computed as follows:.

$$S_{rd,n}(t) = \begin{cases} \int_{t_{0,w}}^{t_{0,d}} (P_e(t) - E_r(t)) dt, & if \ \int_{t_{0,w}}^{t_{0,d}} (P_e(t) - E_r(t)) dt \leq 0 \\ 0, & if \ \int_{t_{0,w}}^{t_{0,d}} (P_e(t) - E_r(t)) dt > 0 \end{cases}$$

(7)

$$S_{rd,n} = \max \left(\left| S_{rd,n}(t) \right| \right) \tag{8}$$

Where t is the time step (d), $t_{0,w}$ is the day at the end of the wet period when the storage deficits are zero but $P_e(t) - E_r(t) < 0$, and $t_{0,d}$ is the day when storage deficits return to zero again after the begin of the next wet period when the water supply exceeds canopy water demand, i.e., $\left(P_e(t) - E_r(t) \right) > 0$. Any cumulative precipitation surplus is assumed to be drained from

225   root zone and released from the system either directly as streamflow or via recharge of the groundwater.

The Gumbel extreme value distribution (Gumbel, 1941) was previously used for estimating the root zone storage capacity through the water balance approach by several other studies (Gao et al., 2014; Nijzink et al., 2016a; de Boer-Euser et al., 2016; Bouaziz et al., 2020, 2022; Hrachowitz et al., 2021). Based on fitting the Gumbel distribution to the maximum annual storage deficits for all n years during one of the four time periods $t_1 - t_4$, the root zone storage capacity $S_{umax,WB}$ can be derived from

230   various return periods of the sequence of n maximum annual storage deficits S_{rd}. Previous studies suggested that vegetation develops root zone storage capacities large enough to survive in dry spells with return periods of $\sim 20 - 40$ years (Gao et al., 2014; deBoer-Euser et al., 2016; Wang-Erlandsson et al., 2016; Hrachowitz et al., 2021). Therefore, we define $S_{umax,WB}$ here as the maximum storage deficit in a 40-year period so that $S_{umax,WB} = S_{rd,40yr}$.

Using the above water balance based method, we determine $S_{umax,WB}$ for the entire study period $1953 - 2022$ ($S_{umax,WB,T}$) as

235   well as individually for the four time periods $t_1 - t_4$ ($S_{umax,WB,t}$) to quantify potential fluctuations of root zone storage capacity reflecting the adaptation to changing climatic conditions.

4.3 Hydrological model

4.3.1 Model architecture

240   Loosely based on the flexible DYNAMITE modular modelling framework (e.g. Hrachowitz et al., 2014), we here used a semi-distributed, process-based model, that has previously been successfully implemented and tested for the Neckar study basin (Wang et al., 2023) and for many other contrasting environments world-wide (e.g. Prenner et al., 2018; Hulsman et al., 2021a, c; Hanus et al., 2021; Bouaziz et al., 2022). Briefly, this hydrological model consists of three parallel hydrological response units (HRU), i.e. forest, grass/cropland and wetland, which are linked through a common storage component representing the

245   groundwater system (Fig. 5). The classification into the three HRUs was based on the metric Height-above-nearest-drainage (HAND; Gharari et al., 2011) and land cover similar to previous studies (e.g. Gao et al., 2014a; Gharari et al., 2014; Nijzink et al., 2016b; Bouaziz et al 2021). The model was further spatially discretized by a stratification into 100m-elevation bands for a more detailed representation of the snow storage (S_{snow}) and finally implemented in parallel, i.e. individually for each of the three precipitation zones P1 – P3 to balance to a certain degree spatial differences in precipitation with computational

250   requirements. Rain (P_{rain}) and melt water (M_{snow}) from the different elevation zones were aggregated according to their

associated spatial weights in each elevation zone as further input to the subsequent layers of the model in each HRU. The outflows from each HRU in each precipitation zone as well as finally the outflows from each precipitation zone were likewise aggregated according to their respective spatial weights to represent the catchment aggregated outflows. While the three HRU's are characterized by distinct parameters that reflect their respective functioning, the parameters between the individual zones P1 – P3 were, in the spirit of model parsimony, kept the same in what is elsewhere referred to as a distributed moisture accounting approach (e.g. Ajami et al., 2004; Fenicia et al., 2008; Euser et al., 2015). Overall, the model consists of snow (S_{snow}), interception (S_i), unsaturated root zone (S_u), fast responding (S_f) and slow responding storage (S_s) components for each HRU and precipitation zone. The maximum storage volume in the unsaturated root zone component in each HRU is defined by the corresponding calibration parameters $S_{umax,F}$, $S_{umax,G}$ and $S_{umax,W}$, respectively. The catchment average $S_{umax,cal}$ is then inferred by aggregating these parameters according to their spatial weights. Water can be released from unsaturated root zones as combined soil evaporation and transpiration flux E_t (mm d^{-1}) which is a frequently applied way to represent vegetation water stress (e.g., Bouaziz et al., 2021, Gharari et al., 2013; Gao et al., 2014a). The equations of the model are provided as Table S1 in the Supplementary Material and more detailed descriptions of the model are provided by Wang et al. (2023) and other earlier implementations referred to above.

4.3.2 Model calibration

The model was run with a daily time step and has 18 calibration parameters. Briefly, the model parameters were calibrated by using the Borg_MOEA algorithm (Borg Multi-objective evolutionary algorithm; Hadka and Reed, 2013) and based on uniform prior distributions (Supplementary Material Table. S2). To best reflect different aspects of the hydrograph, including high flows, low flows and the partitioning of precipitation into runoff and evaporation, the parameters are calibrated using a multi-criteria approach that includes 7 objective functions as performance metrics $E_{Q,n}$ (Table 3). There are multiple ways to deal with sets of pareto front solutions as in detail described by e.g. Efstratiadis and Koutsoyiannis (2010) or Gharari et al. (2013). We chose to use all solutions on the Pareto front to obtain a conservative estimate of uncertainty. The 7 performance metrics were subsequently also combined into an overall performance metric based on the Euclidian distance (D_E), where $D_E = 1$ indicates a perfect fit. To find a somewhat balanced solution in absence of more detailed information all individual performance metrics were here equally weighted (e.g., Hrachowitz et al., 2021; Hulsman et al., 2021c; Wang et al., 2023):

$$D_E = 1 - \sqrt{\frac{\sum_{n=1}^{N}\left(1 - E_{Q,n}\right)^2}{N}} \qquad (9)$$

where $N = 7$ is the number of performance metrics with respect to stream flow ($E_{Q,n}$). Note that the different units and thus different magnitudes of residuals in the individual performance metrics introduce some subjectivity in finding the most balanced overall solution according to D_E (Eq. 9). However, a preliminary sensitivity analysis with varying weights for the individual performance metrics in D_E suggested limited influence on the overall results and is thus not further reported here. In addition, the model was tested for its ability to represent spatial differences in the hydrological response by evaluating it

against streamflow observations in three sub-catchments (C1 – C3) of the upper Neckar catchment without further re-calibration whereby each one of the sub-catchments largely represents the hydrological response from one of the precipitation zones (Fig. 1).

285 The model is calibrated following two distinct calibration scenarios as indicated in Table 2. In the first scenario, the model and thus also $S_{umax,F}$, $S_{umax,G}$ and $S_{umax,W}$ are calibrated over the full length of the 70-yr study period from 1953 – 2022. This reflects the common assumption of a system that is stable over time. By extension, this also implies that the role of vegetation and thus S_{umax} does not change and that vegetation does not adapt to climatic variability. In the second scenario, individual calibration to the four time periods $t_1 – t_4$ allowed to estimate fluctuations in the parameters $S_{umax,F}$, $S_{umax,G}$ and $S_{umax,W}$ between the time 290 periods as indicator of vegetation adaption to changing climatic conditions.

5 Results

5.1 Observed multi-decadal hydroclimatic variability

Based on the initial analysis of water balance data for four sub-time periods, significant differences were observed in the variability of different hydroclimatic indicators over the 1953 – 2022 study period (Fig. 3). While periods t_1 and t_4 were 295 characterized by rather low mean annual precipitation of $\sim$ 870 and 811 mm yr^{-1}, respectively, periods t_2 and t_3 were subject to, on average, higher precipitation with $\sim$ 911 mm yr^{-1}. While summer precipitation remained rather stable over the study period (Fig. 3f), the above was mostly caused by fluctuations in winter precipitation (Fig. 3k). In contrast, potential evaporation E_P has gradually increased by 7% from 836 to 906 mm yr^{-1} (Fig. 3b). Similarly reflecting increases in temperature (Fig. 3b), the annual snowpack and associated snowmelt have continuously decreased from around 98 mm yr^{-1} to around 50 mm yr^{-1} 300 between t_1 and t_4 (Fig. 3c). A slight decrease of the number of days with precipitation from $\sim$ 264 to 251 (Fig. 3d), on average, mostly due to changes in the summer months (Fig. 3n) was accompanied by some rather limited variability in precipitation intensities (Fig. 3e), mostly during winter (Fig. 3j). Overall, the comparatively humid periods $t_1 – t_3$ that were characterized by I_A fluctuating between 0.93 – 0.97 were followed by a markedly more arid period t_4 with $I_A = 1.12$ (Table 2; Figure 6). In response to the multi-decadal variability in I_A, expressed as movement along the x-axis in the Budyko framework, the 305 catchment experienced I_E to vary between 0.56 and 0.59 (Table 2; Figure 6). However, this observed variability was somewhat lower than the variability $I_{E,\omega_T} = 0.55 – 0.61$ that would have been expected based on ω_T. This illustrates that the hydrological response did not consistently follow its long-term trajectory defined by ω_T. Instead, deviations $\Delta I_{E,t_i}$ from the expected positions, and thus values of ω_{t_i} that are different to ω_T, were observed for the individual periods. More specifically, the deviations gradually decreased from $\Delta I_{E,t_1} = 0.01$ in t_1 to $\Delta I_{E,t_4} = - 0.02$ in t_4 (Fig. 6). This systematic shift towards lower (more negative) 310 $\Delta I_{E,t_i}$ and thus also lower ω_{t_i} indicates that at the same I_A a smaller fraction of precipitation is released as evaporation, i.e. I_E, now than at the start of the 70 year study period. Although the magnitude of deviations remains with $\Delta I_{E,t_i} \leq \pm 0.02$ rather minor, similar to what has been recently reported elsewhere (Ibrahim et al., 2024; Tempel et al., 2024), in particular their

systematic shift into one direction implies that changes in the system other than I_A have a visible effect on the hydrological response pattern.

5.2 Root zone storage capacity $S_{umax,WB}$ estimated from water balance data

As the baseline of our study, the annual maximum storage deficits fluctuate between 97 mm in 2022 and 16 mm in 1970 (Fig. 7a). Assuming an adaptation to dry spells with 40-yr return periods the root zone storage capacity over the entire 1953 – 2022 study period (Scenario 1) was estimated to $S_{umax,WB,T}$ = 105 mm (Table 2; Fig. 7b). In the next step, the storage deficits and the associated root zone storage capacity for each period $t_1 – t_4$ was estimated (Scenario 2). S_{umax,WB,t_1} and S_{umax,WB,t_3} for periods t_1 and t_3, respectively, are estimated at the same value of 95 mm. In contrast, and somewhat counterintuitively, the highest value over the study period is found in the wettest period (t_2) and reaches S_{umax,WB,t_2} = 115 mm, while the driest period (t_4) is characterized by S_{umax,WB,t_4} = 100 mm (Table 2; Fig. 7c-j). These pattern suggest that $S_{umax,WB}$ did vary by ~20 mm, equivalent to ~20% throughout the 1953 -2022 period. In contrast to $\Delta I_{E,t_i}$ that was characterized by a systematic shift towards more negative deviations over time, no evidence was found for a systematic, one-directional shift in $S_{umax,WB}$. Instead, $S_{umax,WB}$ evolved following a somewhat cyclic pattern.

5.3 Root zone storage capacity $S_{umax,cal}$ estimated as calibration parameter

5.3.1 Model calibration for 1953 – 2022 (Scenario 1)

The model parameter sets obtained as feasible after calibration over the entire 1953-2022 study period in Scenario 1 reproduce the main features of the hydrological response (Fig. 2d). More specifically, the modelled hydrographs in particular describe well the timing of high flows, albeit somewhat underestimating flow peaks for the best-performing model in terms of the D_E (Eq. 9). The low flows and the shapes of recessions are in general well captured ($NSE_{logQ} = 0.67$). Crucially, the model also reproduces well the other observed stream flow signatures such as the flow duration curves ($NSE_{logFDC} = 0.96$), the autocorrelation function ($NSE_{AC} = 0.99$) as well as the long-term and seasonal runoff coefficients ($NSE_{Cr} = 0.90$, $RE_{Cr,summer} = 0.83$ and $RE_{Cr,winter} = 0.91$). The latter further implies that the modelled long-term actual evaporative fluxes E_A (Fig. 2b) and thus I_{E,ω_T} are, on average, consistent with the observed ones, which can be seen in Figure 6. The model, calibrated on the overall response of the Upper Neckar basin, also exhibited considerable skill to represent spatial differences in the hydrological response by reproducing observed stream flow in the three sub-catchments (C1 – C3) similarly well (Fig. 8) without any further re-calibration. The overall model skill to mimic the hydrological response corresponds well to a similar implementation of the model in the greater study region by Wang et al. (2023). The detailed list of performance metrics is provided in Table S4 in the Supplementary Material.

The model calibration resulted in pronounced differences in the root zone storage capacity parameters for three individual landscape classes. While for forest dominated land it was estimated at $S_{umax,F}$ = 158mm for the best performing model (5th/95th percentile of all feasible solutions: 138–168mm), it reached $S_{umax,G}$ = 95mm (5th/95th: 71–123mm) for grass/cropland and

$S_{umax,W} = 61$ mm for wetland ($5^{th}/95^{th}$: 49–68mm), which reflects differences in vegetation type and position in the landscape (cf. Fan et al., 2017). Remarkably, the catchment root zone storage capacity, estimated by aggregating the individual values according to their areal fractions, came with $S_{umax,cal} = 116$ mm ($5^{th}/95^{th}$: 99–130 mm, Fig. 9a) very close to the estimate $S_{umax,WB}$ = 105 mm that is directly derived from water balance method without any calibration, as described in section 5.2.

5.3.2 Model calibration for individual periods t_1 – t_4 (Scenario 2)

The model parameter sets obtained from the individual calibration for each period t_1 - t_4 reproduce the hydrographs of the corresponding periods as well or slightly better than when using the long-term average parameters from scenario 1 (see detailed performance metrics in Table S4 in the Supplementary Material). In particular, the runoff coefficients could with NSE_{Cr} ~0.86 – 0.91, $RE_{Cr,summer}$ ~ 0.84 – 0.90 and $RE_{Cr,winter}$ ~ 0.88 – 0.92 be rather well mimicked. Similarly, the daily dynamics with NSE_{logQ} ~ 0.63 – 0.72 for the best- performing model of each period. and most other hydrological signatures, could be reproduced marginally better.

The individual calibration over each period t_1 – t_4 resulted in associated differences in the catchment-scale root-zone storage capacity of each period. Based on the best-performing models, the calibrated values varied between low values for t_1 and t_2, with $S_{umax,cal,t_1} = 98$ mm and $S_{umax,cal,t_3} = 99$ mm and higher values for the two other periods with $S_{umax,cal,t2} = 122$ mm and $S_{umax,cal,t_4} = 107$ mm (Table 2; Figure 9a). The magnitudes of S_{umax,cal,t_i} obtained by calibration in the individual time periods t_1 – t_4 are with a difference of 5 mm (~ 5%), on average, very close to S_{umax,WB,t_i} estimated on basis of the water balance for the same periods. Perhaps even more notably the temporal evolution of S_{umax,cal,t_i} and S_{umax,WB,t_i} follows the same sequence over time ($R^2 = 0.95$, $p = 0.05$; Figure 9b).

5.4 Effect of S_{umax} on temporal fluctuation in the trajectories of the Budyko curve

The deviations $\Delta I_{E,O,O'}$ between expected evaporative index $I_{E,O'}$ and observed evaporative index $I_{E,O}$ for all periods t_1 – t_4 become gradually more negative from t_1 ($\Delta I_{E,O,O'}= 0.013$) to t_4 ($\Delta I_{E,O,O'}= -0.020$), which is consistent with   decreases of ω_{t_i} and downward shifts of the associated parametric Budyko curves over time as described in section 5.1. These systematic reductions of $\Delta I_{E,O,O'}$ over the 70-year study period are not reflected in the fluctuations of root zone storage capacities, irrespective of how they were estimated, i.e. S_{umax,WB,t_i} ($p = 0.85$) or S_{umax,cal,t_i} ($p = 0.96$), as illustrated by Figure 10.

The above is further corroborated by comparing the modelled I_E from Scenarios 1 and 2 for each period t_1 – t_4. More specifically, in Figure 11(c) it can be seen that Scenario 1, based on a long-term average, time-invariant $S_{umax,WB,T}$ obtained over the entire 1953 – 2022 period, generates deviations $\Delta I_{E,mT,O'}$ from the expected long-term average $I_{E,O'}$ for each period t_1 – t_4. In this case, the modelled I_E does not follow the expected $I_{E,O'}$. However, it also does not follow the sequence of increasingly negative deviations from 0.013 in t_1 to – 0.020 in t_4 as observed in reality ($\Delta I_{E,O,O'}$). Instead, $\Delta I_{E,mT,O'}$ remains negative for all time periods and fluctuates between $\Delta I_{E,mT,O'} = – 0.005$ and – 0.029 (white boxplots in Fig. 11c). Replacing the time-invariant $S_{umax,WB,T}$ by individual S_{umax,WB,t_i} for each period t_1 – t_4 in Scenario 2, accounts for the different effects of vegetation in the

individual periods. If S_{umax} controlled the observed deviations from expected $I_{E,O'}$, Scenario 2 would generate estimates of $\Delta I_{E,mt_i,O'}$ that are closer to the observed ones than those of Scenario 1. However, no evidence was found for that: the deviations $\Delta I_{Emt,O'}$ obtained by Scenario 2 with time-variable S_{umax} for each period $t_1 - t_4$ are largely indistinguishable (orange boxplots in Fig.11c) from those generated by Scenario 1 with time-invariant S_{umax}. As a consequence, the evaporative index I_E modelled with time-variable S_{umax,WB,t_i} is not found to be closer to the observed I_E for Scenario 2 than for Scenario 1. On the contrary, the deviations $\Delta I_{Em,O}$ from the observed I_E obtained from the time-invariant Scenario 1 are in most time periods, albeit only slightly, less pronounced (Fig. 11d).

5.5 Effect of S_{umax} on stream flow

Corresponding to the above findings, there is no significant difference in modelled average streamflow between Scenario 1, using long-term average S_{umax}, and Scenario 2, using individual S_{umax} values for each time period (Fig. 12d). While the model for both scenarios consistently and similarly underestimates high flows (Q^{5th}, Fig.12a) by ~10%, it overestimates median flow by ~15% with both time-invariant and time-variable S_{umax}, for all time periods (Fig.12b). Interestingly, the low flows are over-predicted by ~ 10 – 20% in the first two periods, while they are under-predicted by up to ~20% in the later periods in both Scenarios (Fig.12c). In addition, it was found that using time variable S_{umax} in Scenario 2 did also not have any discernible effect on seasonal flow pattern (not shown). The fact that both scenarios generate similar estimates over different flow percentiles and, in particular, that the time-variable Scenario 2 reflects the same systematic shift in the ability of the model to reproduce low flows as Scenario 1, suggests, together with the very minor effects of time-variable S_{umax} in Scenario 2 on the model performance metrics, that the adaptation of S_{umax} to changing climatic conditions does not significantly affect the average hydrological response pattern in the Neckar basin.

6 Discussion

6.1 Multi-decadal changes in root zone storage capacity S_{umax}

As Gao et al. (2024) suggested, considering the terrestrial ecosystem structure can improve our understanding of hydrological processes and how the ecosystem can be survived and developed. It is valuable to explore how ecosystems adapt to climatic variability, reflected by fluctuations in S_{umax}, and how this affects on the long-term partitioning of drainage and evaporation and hydrological response. This study is the first to systematically and explicitly quantify how root zone storage capacity S_{umax} changes with changing climatic conditions over time. The values of root zone storage capacity, estimated from both, water balance data and as model calibration parameter, show indeed significant and corresponding fluctuations over multiple decades, varying by up to ±20%. The overall estimated magnitudes fall with S_{umax} ~ 95 – 115 mm well within the range of long-term average values reported previously for the greater region (e.g. Bouaziz et al., 2021; Hrachowitz et al, 2021; Tempel et al., 2024)

and other temperate, humid environments (e.g. Kleidon, 2004; Gao et al., 2014b; de Boer et al., 2016; Wang-Erlandsson et al., 2016; Stocker et al., 2023; van Oorschot et al., 2024).

The values of S_{umax} obtained from both methods are very similar and within an error margin of merely ~5%. In addition, they both follow a comparable change over time. Together, this lends support to the underlying assumption that this temporal evolution of S_{umax} may indeed be a fingerprint of vegetation adaptation to changing climatic conditions. More specifically, as $S_{umax,WB}$ is explicitly based on the estimates of transpiration E_r (Eq. 9), it could be plausibly argued that during specific years merely more water is *used* for E_r but that the size of the water storage volume accessible for roots may not necessarily change. In that case, changes in $S_{umax,WB}$ would not reflect actual changes of the active root system but only in how much water was *used* by them. In contrast, $S_{umax,cal}$ inferred as calibration parameter of a hydrological model does not only regulate transpiration, but, critically, *also* the generation of streamflow. If therefore the active root system did in reality not change and fluctuations in $S_{umax,WB}$ were a mere artifact of changes in water uptake from a fixed-size volume instead of an actual change in of maximum vegetation-accessible subsurface water volumes, fluctuations in $S_{umax,cal}$ would not mirror those of $S_{umax,WB}$ and the use of $S_{umax,WB}$ in the hydrological model would, due to the non-linear character of the flow generation function in the model (Eq. 20 S1 in the Supplementary material), lead to misrepresentations of streamflow dynamics. Yet here, no deteriorations of the model performance with changing S_{umax} were found. Even more, the fact that $S_{umax,WB}$ and $S_{umax,cal}$ are characterized by very similar magnitudes and fluctuations does add further evidence that their evolution over time is a manifestation of vegetation adapting its active root system to changing climatic conditions.

Several previous studies in similar environments found that the root zone storage capacity S_{umax} can decrease by 50% or more after deforestation and that these changes do not only cause reductions in I_E by -0.2 or more, which reflect changes in ω and thus changes of the overall functioning of the system, but also influence hydrological dynamics at short time scales, such as the magnitudes of flow peaks (Nijzink et al., 2016a; Hrachowitz et al.,2021). In contrast to the above studies, the ±20% fluctuations of S_{umax} here did not lead to similarly marked shifts in I_E or ω. This is further corroborated by an analysis of different variables as potential controls on S_{umax} and ΔI_E as shown in Figure 13. Fluctuations of S_{umax} can to a large part be attributed to the variability in the ratio of winter precipitation over summer precipitation (Fig. 13s) as simplified metric for precipitation seasonality. This comes as no surprise, as the computation of $S_{umax,WB}$ is explicitly based on the seasonal water deficit (Eq.7). It merely visualizes that the more precipitation falls in summer, in a time when evaporative demand is highest, the lower S_{umax} needs to be to provide vegetation sufficient and continuous access to water for continuous vegetation transpiration. All other tested variables do not exert any major influence on S_{umax} in the study region. Conversely, it was found that the deviations ΔI_E are largely independent of the seasonality of precipitation (Fig. 13g). Instead, increases in summer E_P are correlated with decreases in ΔI_E (Fig. 13h) and thus with a reduction of E_T. The observed systematic shift towards more negative ΔI_E which indicates proportionally less evaporation thus coincides with the gradually increasing summer E_P over time. This points towards different controls on ΔI_E than on S_{umax} and the potential role of increased vegetation water stress in summer as main driver of ΔI_E. Thus, while there is compelling evidence for fluctuations in S_{umax}, the above illustrates that these changes cannot explain the observed deviations from the expected long-term Budyko trajectory in the study region.

It is also important to note that the temporal fluctuations of both S_{umax} and ΔI_E can be subject to uncertainties. In spite of the findings reported by Han et al. (2020), that for most river catchments world-wide $dS/dt \sim 0$ holds over averaging periods similar to the ones used here ($t_1 - t_4$), this assumption may not completely hold in the study region. In relation with that, we also did not consider potential effects of unobserved groundwater import or export on the long-term water balance (Bouaziz et al., 2018).

As only $< 2\%$ of the study area experienced documented land use change over the $1953 - 2022$ period and no major reservoirs are present upstream of the study basin outlet, we here interpret fluctuations in S_{umax} as a reflection of adaptation of root-systems to changing hydroclimatic conditions. However, some of the fluctuations may be the consequence of land management practices not quantified by available gridded land cover products such as CORINE, including forest thinning (cf. Hrachowitz et al., 2021) or rejuvenation (cf. Teuling and Hoek van Dijke, 2020). In addition, although we here attribute changes in S_{umax} mainly to changes in root systems, these may be complemented by additional effects of changes in vegetation water use due to feedbacks with increases in atmospheric CO_2 (e.g. Berghuijs et al., 2017; Jaramillo et al., 2018a).

6.2 Effect of changing S_{umax} on the representation of stream flow in a model

Reflecting its lack of explanatory power for the changes in ΔI_E, our results correspondingly indicate that signatures of both annual flow, such as the average Q^{5th}, Q^{50th} or Q^{95th} but also of seasonal flow are not better reproduced by the hydrological model when replacing a time-invariant, long-term average S_{umax} by a temporally dynamic S_{umax}. Overall, these results are in contrast to previous studies that quantified the effect of a time variable S_{umax} parameter following deforestation. For example, Nijzink et al. (2016a) reported that adjusting parameter S_{umax} to a lower value does improve a model's ability to reproduce streamflow after deforestation. These findings were strongly supported by Hrachowitz et al. (2021), who found that post-deforestation model recalibration resulted in lower S_{umax} and a significantly better performance compared to using parameters from pre-deforestation calibration. However, our results are also different to those reported by Duethmann et al. (2020), who found that accounting for vegetation dynamics in a model in form of changing surface resistances to vegetation improved the long-term performance of the model. Similarly, Bouaziz et al. (2022), who estimated future S_{umax} based on projected future hydro-climatic conditions. In a somewhat more humid environment, they found that an estimated $\sim 25\%$ future increase of S_{umax} from ~ 170 mm to 226 mm may lead to reductions in mean and maximum annual Q of $\sim 5\%$. More pronounced effects were reported at the intra-annual time scale, with reductions of autumn and winter Q by up to $\sim 15\%$. This was accompanied by up $\sim 15\%$ increases in summer evaporation and 10% decreases in winter groundwater levels. Irrespective of the additional uncertainties in their study introduced by future projections, the much less pronounced effects we found in our analysis are most likely a consequence of the lower absolute magnitude of S_{umax} that remains below 115 mm in the study region. These lower S_{umax} values reflect lower storage requirements in summer, due to a precipitation pattern in the Neckar basin that is more evenly spread throughout the year. In other words, the fact that here $\sim 55 - 60$ % of the annual precipitation falls in summer (Fig. 3f, k) when it is needed most by vegetation due to high E_P, removes the need for larger S_{umax} as water storage buffer to allow vegetation to survive. However, the lower the magnitude of S_{umax}, the more frequently storage deficits can be overcome

by even rather small rainstorms and the less water is (or needs to be) stored. Thus even if the relative changes are similar between Bouaziz et al. (2022) and Tempel et al. (2024) in a somewhat more humid environment and our study, abundant summer precipitation causes absolute S_{umax} fluctuations of less than ±20 mm over time in the Neckar. This in turn limits the influence of the changes on the hydrological response, which has wider implications on the use of models in the Neckar basin and potentially in other temperate regions with similar hydro-climatic characteristics. More specifically, it has been argued that a changing climate will affect the properties of terrestrial hydrological systems (e.g. Stevens et al., 2020). As these properties are represented by typically time-invariant parameters in hydrological or land surface models, accounting for changing system properties with time-variable formulations of parameters may facilitate more reliable predictions. For many model parameters such a time-variable formulation to estimate their future values is not trivial due to frequently insufficient data and a general lack of mechanistic understanding of the underlying processes. The estimation of S_{umax} and its temporal evolution based on observed historical or projected future water balance data opens an opportunity to estimate its magnitude under future conditions for use in models. However, in contrast to the findings in other regions (e.g. Merz et al., 2011) and as discussed above, adapting S_{umax} to changing conditions in the Neckar basin does not lead to improved modelled representations of the hydrological response. It is therefore plausible to assume that the use of a time-variable parameter S_{umax} does not substantially improve future predictions and is thus not necessarily required for at least the next few decades to come and that the use of a long-term average S_{umax}, obtained either by calibration or based on the water balance is sufficient in the Neckar basin and in hydro-climatically similar regions. This in itself is already an interesting finding as it gives modelers process-based evidence that the use of time-invariant S_{umax} as model parameter will be also sufficient for meaningful hydrological predictions in the near future in such an environment. However, it can also be expected that in more arid regions with less summer precipitation and generally higher S_{umax} (see e.g. Gao et al., 2014; Stocker et al., 2023) changes in S_{umax} will play a more prominent role.

7 Conclusions

The catchment-scale root zone storage capacity (S_{umax}) is a critical factor reflecting the moisture exchange between land and atmosphere as well as the hydrological response in terrestrial hydrological systems. However, as a major knowledge gap, it is unclear if S_{umax} at the catchment-scale evolves over time, reflecting vegetation adaptation to changing climatic conditions. As a consequence, it also remains unclear how potential changes in S_{umax} may affect the partitioning of water fluxes and as a consequence, the catchment-scale hydrological response. In this study, for the upper Neckar catchment, based on long-term daily hydrological data (1953 – 2022), we quantify and analyze how S_{umax} dynamically evolves over multiple decades reflecting vegetation adaptation to climate variability and the effects on the hydrological system.

The main findings of our analysis are the following:

(1) S_{umax} has fluctuated by $\pm\ 20\ \%$ between 95 and 115 mm, in response to climatic variability over the 70-year study period.

(2) Estimates of S_{umax} obtained from both methods, i.e. based on water balance data and as model calibration parameter,

respectively, were with differences of ~5% highly consistent with each other and correlated in time ($R^2 = 0.95$, $p = 0.05$).

505 Findings (1) and (2) support the hypothesis that S_{umax}, even in temperate, humid climates such as in the Neckar basin, significantly changes over multiple decades, reflecting vegetation adaptation to climatic variability.

(3) The estimated fluctuations of S_{umax} were inconsistent with the temporal sequence of observed deviations $\Delta I_E \sim \pm 0.02$ from the expected I_E over the study period ($R^2 = 0.02$, $p = 0.85$).

(4) As a consequence, replacing a long-term average, time-invariant parameter S_{umax} in a hydrological model with a time

510 variable formulation of S_{umax} does not lead to a better representation of the observed ΔI_E. Based on (3) and (4), the hypothesis that S_{umax} affects the long-term partitioning of drainage and evaporation and thus controls deviations ΔI_E from the catchment-specific trajectory in the Budyko space therefore needs to be rejected for the Neckar basin.

(5) Replacing time-invariant S_{umax} with a time-variable S_{umax} in the hydrological model leads to only very minor improvements of the model to reproduce streamflow dynamics. The hypothesis that a time-dynamic implementation of S_{umax} improves the

515 representation of streamflow in the hydrological therefore also needs to be rejected for the Neckar basin.

Overall, our study is the first to systematically document the temporal evolution of S_{umax}, and although limited to the Neckar basin, it provides clear quantitative evidence that S_{umax} can significantly change over multiple decades reflecting vegetation adaptation to climate variability. However, these changes do not cause deviations from the long-term average Budyko curve under changing climatic conditions. This implies that the temporal evolution of S_{umax} does not control variation in the

520 partitioning of water fluxes and has no significant effects on fundamental hydrological response characteristics of the Upper Neckar basin. As the use of time-variable S_{umax} over the 70-year study period does not improve performance of the hydrological model, it can plausibly be assumed that in the study region the use of time-invariant S_{umax} as model parameter will be sufficient for meaningful predictions over at least the next few decades.

525 *Code availability.* The model codes underlying this paper will be available online in the 4TU data repository (DOI: 10.4121/922d30de-a26b-4c81-8644-ad036182239c). The equations used in the model are described in supplement.

Data availability. The meteorological and hydrological data used in this study can be obtained from German Weather Service (DWD) and the German Federal Institute of Hydrology (BfG).

530

Author contributions. SW, MH and GS designed the study, SW executed the experiments, all authors contributed to general idea, the discussion and writing of the manuscript.

Competing interests. At least one of the (co-) author is a member of the editorial board of Hydrology and Earth System Science.

535

Acknowledgements. We gratefully acknowledge financial support from China Scholarship Council (CSC).

540 **References**

AghaKouchak, A., Feldman, D., Hoerling, M., Huxman, T., and Lund, J.: Water and climate: Recognize anthropogenic drought, Nature, 524, 409-411, https://doi.org/10.1038/524409a, 2015.

Ajami, N. K., Gupta, H., Wagener, T., and Sorooshian, S.: Calibration of a semi-distributed hydrologic model for streamflow estimation along a river system, Journal of hydrology, 298, 112-135, https://doi.org/10.1016/j.jhydrol.2004.03.033, 2004.

545 Alila, Y., Kuraś, P. K., Schnorbus, M., and Hudson, R.: Forests and floods: A new paradigm sheds light on age-old controversies, Water Resources Research, 45, 2009.

Allen, C. D., Macalady, A. K., Chenchouni, H., Bachelet, D., McDowell, N., Vennetier, M., Kitzberger, T., Rigling, A., Breshears, D. D., and Hogg, E. T.: A global overview of drought and heat-induced tree mortality reveals emerging climate change risks for forests, Forest ecology and management, 259, 660-684, https://doi.org/10.1029/2008WR007207, 2010.

550 Bahremand, A. and Hosseinalizadeh, M.: Development of conceptual hydrological FLEX-Topo model for loess watersheds influenced by piping and tunnel erosion in Golestan Province of Iran, Journal of Water and Soil Conservation, 29, 115-133, https://doi.org/10.22069/jwsc.2022.20050.3544, 2022.

Berghuijs, W. R., Larsen, J. R., Van Emmerik, T. H., and Woods, R. A.: A global assessment of runoff sensitivity to changes in precipitation, potential evaporation, and other factors, Water Resources Research, 53, 8475-8486, 555 https://doi.org/10.1002/2017WR021593, 2017.

Bouaziz, L., Weerts, A., Schellekens, J., Sprokkereef, E., Stam, J., Savenije, H., and Hrachowitz, M.: Redressing the balance: quantifying net intercatchment groundwater flows, Hydrology and Earth System Sciences, 22, 6415-6434, https://doi.org/10.5194/hess-22-6415-2018, 2018.

Bouaziz, L. J., Steele-Dunne, S. C., Schellekens, J., Weerts, A. H., Stam, J., Sprokkereef, E., Winsemius, H. H., Savenije, H. 560 H., and Hrachowitz, M.: Improved understanding of the link between catchment-scale vegetation accessible storage and satellite-derived Soil Water Index, Water Resources Research, 56, e2019WR026365, https://doi.org/10.1029/2019WR026365, 2020.

Bouaziz, L. J., Aalbers, E. E., Weerts, A. H., Hegnauer, M., Buiteveld, H., Lammersen, R., Stam, J., Sprokkereef, E., Savenije, H. H., and Hrachowitz, M.: Ecosystem adaptation to climate change: the sensitivity of hydrological predictions to time-565 dynamic model parameters, Hydrology and Earth System Sciences, 26, 1295-1318, https://doi.org/10.5194/hess-26-1295-2022, 2022.

Bouaziz, L. J., Fenicia, F., Thirel, G., de Boer-Euser, T., Buitink, J., Brauer, C. C., De Niel, J., Dewals, B. J., Drogue, G., and Grelier, B.: Behind the scenes of streamflow model performance, Hydrology and Earth System Sciences, 25, 1069-1095, https://doi.org/10.5194/hess-25-1069-2021, 2021.

570   Brath, A., Montanari, A., and Moretti, G.: Assessing the effect on flood frequency of land use change via hydrological simulation (with uncertainty), Journal of hydrology, 324, 141-153, https://doi.org/10.1016/j.jhydrol.2005.10.001, 2006.

Brown, D. G., Johnson, K. M., Loveland, T. R., and Theobald, D. M.: Rural land-use trends in the conterminous United States, 1950–2000, Ecological applications, 15, 1851-1863, https://doi.org/10.1890/03-5220, 2005a.

Budyko, M. I., Climate and Life, 508 pp., Academic Press, New York, 1974.

575   Coenders-Gerrits, A. M. J., Van der Ent, R. J., Bogaard, T. A., Wang-Erlandsson, L., Hrachowitz, M., and Savenije, H. H. G.: Uncertainties in transpiration estimates, Nature, 506(7487), E1-E2, https://doi.org/10.1038/nature12925, 2014.

de Boer-Euser, T., McMillan, H. K., Hrachowitz, M., Winsemius, H. C., and Savenije, H. H.: Influence of soil and climate on root zone storage capacity, Water Resources Research, 52, 2009-2024, https://doi.org/10.1002/2015WR018115, 2016.

Donohue, R., Roderick, M., and McVicar, T. R.: On the importance of including vegetation dynamics in Budyko's hydrological
580   model, Hydrology and Earth System Sciences, 11, 983-995, https://doi.org/10.5194/hess-11-983-2007, 2007.

Donohue, R. J., Roderick, M. L., and McVicar, T. R.: Roots, storms and soil pores: Incorporating key ecohydrological processes into Budyko's hydrological model, Journal of Hydrology, 436, 35-50, https://doi.org/10.1016/j.jhydrol.2012.02.033, 2012.

Dralle, D. N., Hahm, W. J., Chadwick, K. D., McCormick, E., and Rempe, D. M.: Accounting for snow in the estimation of
585   root zone water storage capacity from precipitation and evapotranspiration fluxes, Hydrology and Earth System Sciences, 25, 2861-2867, https://doi.org/10.5194/hess-25-2861-2021, 2021.

Duethmann, D., Blöschl, G., & Parajka, J.: Why does a conceptual hydrological model fail to correctly predict discharge changes in response to climate change?. Hydrology and Earth System Sciences, 24(7), 3493-3511, https://doi.org/10.5194/hess-24-3493-2020, 2020.

590   Efstratiadis, A. and Koutsoyiannis, D.: One decade of multi-objective calibration approaches in hydrological modelling: a review, Hydrological Sciences Journal–Journal Des Sciences Hydrologiques, 55, 58-78, https://doi.org/10.1080/02626660903526292, 2010.

Ellison, D., Pokorný, J., and Wild, M.: Even cooler insights: On the power of forests to (water the Earth and) cool the planet, Global Change Biology, 30, e17195, https://doi.org/10.1111/gcb.17195, 2024.

595   Euser, T., Hrachowitz, M., Winsemius, H. C., and Savenije, H. H.: The effect of forcing and landscape distribution on performance and consistency of model structures, Hydrological Processes, 29, 3727-3743, https://doi.org/10.1002/hyp.10445, 2015.

Fenicia, F., Savenije, H. H., and Avdeeva, Y.: Anomaly in the rainfall-runoff behaviour of the Meuse catchment. Climate, land-use, or land-use management?, Hydrology and Earth System Sciences, 13, 1727-1737, https://doi.org/10.5194/hess-13-
600   1727-2009, 2009.

Fenicia, F., Savenije, H. H., Matgen, P., & Pfister, L.: Understanding catchment behavior through stepwise model concept improvement. Water Resources Research, 44, https://doi.org/10.1029/2006WR005563, 2008.

Fu, B.: On the calculation of the evaporation from land surface [in Chinese], Scientia Atmospherica Sinica, 5, 23-31, 1981.

Gao, H., Hrachowitz, M., Fenicia, F., Gharari, S., and Savenije, H.: Testing the realism of a topography-driven model (FLEX-Topo) in the nested catchments of the Upper Heihe, China, Hydrology and Earth System Sciences, 18, 1895-1915, https://doi.org/10.5194/hess-18-1895-2014, 2014a.

Gao, H., Hrachowitz, M., Schymanski, S., Fenicia, F., Sriwongsitanon, N., and Savenije, H.: Climate controls how ecosystems size the root zone storage capacity at catchment scale, Geophysical Research Letters, 41, 7916-7923, https://doi.org/10.1002/2014GL061668, 2014b.

Gao, H., Hrachowitz, M., Wang-Erlandsson, L., Fenicia, F., Xi, Q., Xia, J., Shao, W., Sun, G., and Savenije, H.: Root zone in the Earth system, EGUsphere [preprint], https://doi.org/10.5194/egusphere-2024-332, 2024.

Gentine, P., D'Odorico, P., Lintner, B. R., Sivandran, G., and Salvucci, G.: Interdependence of climate, soil, and vegetation as constrained by the Budyko curve, Geophysical Research Letters, 39, https://doi.org/10.1029/2012GL053492, 2012.

Gharari, S., Hrachowitz, M., Fenicia, F., and Savenije, H.: Hydrological landscape classification: investigating the performance of HAND based landscape classifications in a central European meso-scale catchment, Hydrology and Earth System Sciences, 15, 3275-3291, https://doi.org/10.5194/hess-15-3275-2011, 2011.

Gharari, S., Hrachowitz, M., Fenicia, F., and Savenije, H.: An approach to identify time consistent model parameters: sub-period calibration, Hydrology and Earth System Sciences, 17, 149-161, https://doi.org/10.5194/hess-17-149-2013, 2013.

Gharari, S., Hrachowitz, M., Fenicia, F., Gao, H., and Savenije, H.: Using expert knowledge to increase realism in environmental system models can dramatically reduce the need for calibration, Hydrology and Earth System Sciences, 18, 4839-4859, https://doi.org/10.5194/hess-18-4839-2014, 2014.

Goovaerts, P.: Geostatistical approaches for incorporating elevation into the spatial interpolation of rainfall, Journal of hydrology, 228, 113-129, https://doi.org/10.1016/S0022-1694(00)00144-X, 2000.

Gumbel, E. J.: The return period of flood flows, The annals of mathematical statistics, 12, 163-190, https://www.jstor.org/stable/2235766, 1941.

Guswa, A. J.: The influence of climate on root depth: A carbon cost-benefit analysis, Water Resources Research, 44, W02427, https://doi.org/10.1029/2007WR006384, 2008.

Hadka, D. and Reed, P.: Borg: An auto-adaptive many-objective evolutionary computing framework, Evolutionary computation, 21, 231-259, https://doi.org/10.1029/2007WR006384, 2013.

Han, S. and Tian, F.: A review of the complementary principle of evaporation: from the original linear relationship to generalized nonlinear functions, Hydrology and Earth System Sciences, 24, 2269-2285, https://doi.org/10.5194/hess-24-2269-2020, 2020.

Hanus, S., Hrachowitz, M., Zekollari, H., Schoups, G., Vizcaino, M., and Kaitna, R.: Future changes in annual, seasonal and monthly runoff signatures in contrasting Alpine catchments in Austria, Hydrology and Earth System Sciences, 25, 3429-3453, https://doi.org/10.5194/hess-25-3429-2021, 2021.

Hoek van Dijke, A. J., Herold, M., Mallick, K., Benedict, I., Machwitz, M., Schlerf, M., Pranindita, A., Theeuwen, J. J., Bastin, J.-F., and Teuling, A. J.: Shifts in regional water availability due to global tree restoration, Nature Geoscience, 15, 363-368,

https://doi.org/10.1038/s41561-022-00935-0, 2022.

Hrachowitz, M. and Weiler, M.: Uncertainty of precipitation estimates caused by sparse gauging networks in a small, mountainous watershed, Journal of Hydrologic Engineering, 16, 460-471, https://doi.org/10.1061/(ASCE)HE.1943-5584.0000331, 2011.

Hrachowitz, M., Savenije, H., Bogaard, T., Tetzlaff, D., and Soulsby, C.: What can flux tracking teach us about water age distribution patterns and their temporal dynamics? Hydrology and Earth System Sciences, 17, 533-564, https://doi.org/10.5194/hess-17-533-2013, 2013.

Hrachowitz, M., Stockinger, M., Coenders-Gerrits, M., van der Ent, R., Bogena, H., Lücke, A., and Stumpp, C.: Reduction of vegetation-accessible water storage capacity after deforestation affects catchment travel time distributions and increases young water fractions in a headwater catchment, Hydrology and earth system sciences, 25, 4887-4915, https://doi.org/10.5194/hess-25-4887-2021, 2021.

Hrachowitz, M., Fovet, O., Ruiz, L., Euser, T., Gharari, S., Nijzink, R., Freer, J., Savenije, H., and Gascuel-Odoux, C.: Process consistency in models: The importance of system signatures, expert knowledge, and process complexity, Water resources research, 50, 7445-7469, https://doi.org/10.1002/2014WR015484, 2014.

Hulsman, P., Hrachowitz, M., and Savenije, H. H.: Improving the representation of long-term storage variations with conceptual hydrological models in data-scarce regions, Water Resources Research, 57, e2020WR028837, https://doi.org/10.1029/2020WR028837, 2021a.

Hulsman, P., Savenije, H. H., and Hrachowitz, M.: Learning from satellite observations: increased understanding of catchment processes through stepwise model improvement, Hydrology and Earth System Sciences, 25, 957-982, https://doi.org/10.5194/hess-25-957-2021, 2021c.

Ibrahim, M., Coenders-Gerrits, M., van der Ent, R., & Hrachowitz, M.: Catchments do not strictly follow Budyko curves over multiple decades but deviations are minor and predictable. Hydrology and Earth System Sciences Discussions, 2024, 1-27, https://doi.org/10.5194/hess-2024-120, 2024.

Jaramillo, F. and Destouni, G.: Developing water change spectra and distinguishing change drivers worldwide, Geophysical Research Letters, 41, 8377-8386, https://doi.org/10.1002/2014GL061848, 2014.

Jaramillo, F., Cory, N., Arheimer, B., Laudon, H., Van Der Velde, Y., Hasper, T. B., Teutschbein, C., and Uddling, J.: Dominant effect of increasing forest biomass on evapotranspiration: interpretations of movement in Budyko space, Hydrology and Earth System Sciences, 22, 567-580, https://doi.org/10.5194/hess-22-567-2018, 2018a.

Jasechko, S.: Plants turn on the tap, Nature Climate Change, 8, 562-563, https://doi.org/10.1038/s41558-018-0212-z, 2018.

Kleidon, A.: Beyond Gaia: Thermodynamics of Life and Earth System Functioning. Climatic Change, 66, 271–319, https://doi.org/10.1023/B:CLIM.0000044616.34867.ec, 2004.

Laio, F., Porporato, A., Ridolfi, L., and Rodriguez-Iturbe, I.: Plants in water-controlled ecosystems: active role in hydrologic processes and response to water stress: II. Probabilistic soil moisture dynamics, Advances in water resources, 24, 707-723, https://doi.org/10.1016/S0309-1708(01)00005-7, 2001.

Liancourt, P., Sharkhuu, A., Ariuntsetseg, L., Boldgiv, B., Helliker, B. R., Plante, A. F., Petraitis, P. S., and Casper, B. B.: Temporal and spatial variation in how vegetation alters the soil moisture response to climate manipulation, Plant and Soil, 351, 249-261, https://doi.org/10.1007/s11104-011-0956-y, 2012.

675 Lloyd, C.: Assessing the effect of integrating elevation data into the estimation of monthly precipitation in Great Britain, Journal of Hydrology, 308, 128-150, https://doi.org/10.1016/j.jhydrol.2004.10.026, 2005.

McCormick, E. L., Dralle, D. N., Hahm, W. J., Tune, A. K., Schmidt, L. M., Chadwick, K. D., and Rempe, D. M.: Widespread woody plant use of water stored in bedrock, Nature, 597, 225-229, https://doi.org/10.1038/s41586-021-03761-3, 2021.

McMurtrie, R. E., Iversen, C. M., Dewar, R. C., Medlyn, B. E., Näsholm, T., Pepper, D. A., and Norby, R. J.: Plant root
680 distributions and nitrogen uptake predicted by a hypothesis of optimal root foraging, Ecology and Evolution, 2, 1235-1250, https://doi.org/10.1002/ece3.266, 2012.

Merz, R., Parajka, J., and Blöschl, G.: Time stability of catchment model parameters: Implications for climate impact analyses, Water resources research, 47, https://doi.org/10.1029/2010WR009505, 2011.

Mianabadi, A., Coenders-Gerrits, M., Shirazi, P., Ghahraman, B., and Alizadeh, A.: A global Budyko model to partition
685 evaporation into interception and transpiration, Hydrology and Earth System Sciences, 23, 4983-5000, https://doi.org/10.5194/hess-23-4983-2019, 2019.

Miralles, D. G., Brutsaert, W., Dolman, A. J., & Gash, J. H.: On the use of the term "evapotranspiration", Water Resources Research, 56, e2020WR028055, https://doi.org/10.1029/2020WR028055, 2020.

Nijzink, R., Almeida, S., Pechlivanidis, I., Capell, R., Gustafssons, D., Arheimer, B., Parajka, J., Freer, J., Han, D., and
690 Wagener, T.: Constraining conceptual hydrological models with multiple information sources, Water Resources Research, 54, 8332-8362, https://doi.org/10.1029/2017WR021895, 2018.

Nijzink, R., Hutton, C., Pechlivanidis, I., Capell, R., Arheimer, B., Freer, J., Han, D., Wagener, T., McGuire, K., and Savenije, H.: The evolution of root-zone moisture capacities after deforestation: a step towards hydrological predictions under change? Hydrology and Earth System Sciences, 20, 4775-4799, https://doi.org/10.5194/hess-20-4775-2016, 2016a.

695 Nijzink, R. C., Samaniego, L., Mai, J., Kumar, R., Thober, S., Zink, M., Schäfer, D., Savenije, H. H., and Hrachowitz, M.: The importance of topography-controlled sub-grid process heterogeneity and semi-quantitative prior constraints in distributed hydrological models, Hydrology and Earth System Sciences, 20, 1151-1176, https://doi.org/10.5194/hess-20-1151-2016, 2016b.

Ol'Dekop, E.: On evaporation from the surface of river basins, Transactions on meteorological observations, 4, 200, 1911.

700 Oudin, L., Andréassian, V., Lerat, J., and Michel, C.: Has land cover a significant impact on mean annual streamflow? An international assessment using 1508 catchments, Journal of hydrology, 357, 303-316, https://doi.org/10.1016/j.jhydrol.2008.05.021, 2008.

Oudin, L., Hervieu, F., Michel, C., Perrin, C., Andréassian, V., Anctil, F., and Loumagne, C.: Which potential evapotranspiration input for a lumped rainfall–runoff model?: Part 2—Towards a simple and efficient potential
705 evapotranspiration model for rainfall–runoff modelling, Journal of hydrology, 303, 290-306,

https://doi.org/10.1016/j.jhydrol.2004.08.026, 2005.

Prenner, D., Kaitna, R., Mostbauer, K., and Hrachowitz, M.: The value of using multiple hydrometeorological variables to predict temporal debris flow susceptibility in an alpine environment, Water Resources Research, 54, 6822-6843, https://doi.org/10.1029/2018WR022985, 2018.

710 Reaver, N. G., Kaplan, D. A., Klammler, H., and Jawitz, J. W.: Theoretical and empirical evidence against the Budyko catchment trajectory conjecture, Hydrology and Earth System Sciences, 26, 1507-1525, https://doi.org/10.5194/hess-26-1507-2022, 2022.

Roberts, K. J., Dietrich, J. C., Wirasaet, D., Pringle, W. J., and Westerink, J. J.: Dynamic load balancing for predictions of storm surge and coastal flooding, Environmental Modelling & Software, 140, 105045, 715 https://doi.org/10.1016/j.envsoft.2021.105045, 2021.

Roderick, M. L. and Farquhar, G. D.: A simple framework for relating variations in runoff to variations in climatic conditions and catchment properties, Water Resources Research, 47, https://doi.org/10.1029/2010WR009826, 2011.

Rodríguez-Iturbe, I. and Porporato, A.: Ecohydrology of water-controlled ecosystems: soil moisture and plant dynamics, Cambridge University Press, 2007.

720 Roodari, A., Hrachowitz, M., Hassanpour, F., and Yaghoobzadeh, M.: Signatures of human intervention–or not? Downstream intensification of hydrological drought along a large Central Asian river: the individual roles of climate variability and land use change, Hydrology and Earth System Sciences, 25, 1943-1967, https://doi.org/10.5194/hess-25-1943-2021, 2021.

Sadayappan, K., Keen, R., Jarecke, K. M., Moreno, V., Nippert, J. B., Kirk, M. F., Sullivan, P. L., and Li, L.: Drier streams despite a wetter climate in woody-encroached grasslands, Journal of Hydrology, 627, 130388, 725 https://doi.org/10.1016/j.jhydrol.2023.130388, 2023.

Savenije, H. H.: The importance of interception and why we should delete the term evapotranspiration from our vocabulary, Hydrological Processes, 18, 1507-1511, https://doi.org/10.1002/hyp.5563, 2004.

Savenije, H. H. G. and Hrachowitz, M.: HESS Opinions Catchments as meta-organisms – a new blueprint for hydrological modelling, Hydrol. Earth Syst. Sci., 21, 1107–1116, https://doi.org/10.5194/hess-21-1107-2017, 2017

730 Schenk, H. J. and Jackson, R. B.: Rooting depths, lateral root spreads and below-ground/above-ground allometries of plants in water-limited ecosystems, Journal of Ecology, 480-494, https://www.jstor.org/stable/3072232, 2002.

Schreiber, P.: Über die Beziehungen zwischen dem Niederschlag und der Wasserführung der Flüsse in Mitteleuropa, Z. Meteorol, 21, 441-452, 1904.

Scrivner, C. and Ruppert, D.: Thickness of soil solum as a parameter of plant-available water storage capacity in soils underlain 735 by carbonate rocks, https://hdl.handle.net/10355/91873, 1970.

Sivandran, G. and Bras, R. L.: Identifying the optimal spatially and temporally invariant root distribution for a semiarid environment, Water Resources Research, 48, https://doi.org/10.1029/2012WR012055, 2012.

Sivandran, G. and Bras, R. L.: Dynamic root distributions in ecohydrological modeling: A case study at Walnut Gulch Experimental Watershed, Water Resources Research, 49, 3292-3305, https://doi.org/10.1002/wrcr.20245, 2013.

740   Speich, M. J., Lischke, H., and Zappa, M.: Testing an optimality-based model of rooting zone water storage capacity in temperate forests, Hydrology and Earth System Sciences, 22, 4097-4124, https://doi.org/10.5194/hess-22-4097-2018, 2018.

Sriwongsitanon, N., Jandang, W., Williams, J., Suwawong, T., Maekan, E., and Savenije, H. H.: Using normalised difference infrared index patterns to constrain semi-distributed rainfall–runoff models in tropical nested catchments, Hydrology and Earth System Sciences, 27, 2149-2171, https://doi.org/10.5194/hess-27-2149-2023, 2023.

745   Stephens, C. M., Lall, U., Johnson, F., and Marshall, L. A.: Landscape changes and their hydrologic effects: Interactions and feedbacks across scales, Earth-Science Reviews, 212, 103466, https://doi.org/10.1016/j.earscirev.2020.103466, 2021.

Stevens, J. T., Boisramé, G. F., Rakhmatulina, E., Thompson, S. E., Collins, B. M., & Stephens, S. L.: Forest vegetation change and its impacts on soil water following 47 years of managed wildfire, Ecosystems, 23, 1547-1565, https://doi.org/10.1007/s10021-020-00489-5, 2020.

750   Stocker, B. D., Tumber-Dávila, S. J., Konings, A. G., Anderson, M. C., Hain, C., and Jackson, R. B.: Global patterns of water storage in the rooting zones of vegetation, Nature geoscience, 16(3), 250-256, https://doi.org/10.1038/s41561-023-01125-2, 2023

Tempel, N. T., Bouaziz, L., Taormina, R., van Noppen, E., Stam, J., Sprokkereef, E., and Hrachowitz, M.: Vegetation Response to Climatic Variability: Implications for Root Zone Storage and Streamflow Predictions, EGUsphere [preprint],
755   https://doi.org/10.5194/egusphere-2024-115, 2024

Teuling, A. J. and Hoek van Dijke, A. J.: Forest age and water yield, Nature, 578, E16-E18, https://doi.org/10.1038/s41586-020-1941-5, 2020.

Teuling, A. J., De Badts, E. A., Jansen, F. A., Fuchs, R., Buitink, J., Hoek van Dijke, A. J., and Sterling, S. M.: Climate change, reforestation/afforestation, and urbanization impacts on evapotranspiration and streamflow in Europe, Hydrology and Earth
760   System Sciences, 23, 3631-3652, https://doi.org/10.5194/hess-23-3631-2019, 2019.

Tixeront, J.: Prévision des apports des cours d'eau, Publication de l'Association internationale d'hydrologie scientifique, 118-126, http://pascal-francis.inist.fr/vibad/index.php?action=getRecordDetail&idt=19271864, 1964.

Tong, R., Parajka, J., Széles, B., Greimeister-Pfeil, I., Vreugdenhil, M., Komma, J., Valent, P., and Blöschl, G.: The value of satellite soil moisture and snow cover data for the transfer of hydrological model parameters to ungauged sites, Hydrology and
765   Earth System Sciences, 26, 1779-1799, https://doi.org/10.5194/hess-26-1779-2022, 2022.

Van der Velde, Y., Vercauteren, N., Jaramillo, F., Dekker, S. C., Destouni, G., and Lyon, S. W.: Exploring hydroclimatic change disparity via the Budyko framework, Hydrological Processes, 28, 4110-4118, https://doi.org/10.1002/hyp.9949, 2014.

Van Loon, A. F., Stahl, K., Di Baldassarre, G., Clark, J., Rangecroft, S., Wanders, N., Gleeson, T., Van Dijk, A. I., Tallaksen, L. M., and Hannaford, J.: Drought in a human-modified world: reframing drought definitions, understanding, and analysis
770   approaches, Hydrology and Earth System Sciences, 20, 3631-3650, https://doi.org/10.5194/hess-20-3631-2016, 2016.

van Oorschot, F., van der Ent, R. J., Hrachowitz, M., and Alessandri, A.: Climate-controlled root zone parameters show potential to improve water flux simulations by land surface models, Earth System Dynamics, 12, 725-743, https://doi.org/10.5194/esd-12-725-2021, 2021.

van Oorschot, F., van der Ent, R. J., Alessandri, A., & Hrachowitz, M.: Influence of irrigation on root zone storage capacity estimation. Hydrology and Earth System Sciences, 28(10), 2313-2328, https://doi.org/10.5194/hess-28-2313-2024, 2024.

Verdin, K.L.: Hydrologic Derivatives for Modeling and Applications (HDMA) database: U.S. Geological Survey data release, https://doi.org/10.5066/F7S180ZP, 2017.

Wagener, T., McIntyre, N., Lees, M., Wheater, H., and Gupta, H.: Towards reduced uncertainty in conceptual rainfall-runoff modelling: Dynamic identifiability analysis, Hydrological processes, 17, 455-476, https://doi.org/10.1002/hyp.1135, 2003.

Wang-Erlandsson, L., Bastiaanssen, W. G., Gao, H., Jägermeyr, J., Senay, G. B., Van Dijk, A. I., Guerschman, J. P., Keys, P. W., Gordon, L. J., and Savenije, H. H.: Global root zone storage capacity from satellite-based evaporation, Hydrology and Earth System Sciences, 20, 1459-1481, https://doi.org/10.5194/hess-20-1459-2016, 2016.

Wang, S., Hrachowitz, M., Schoups, G., and Stumpp, C.: Stable water isotopes and tritium tracers tell the same tale: no evidence for underestimation of catchment transit times inferred by stable isotopes in StorAge Selection (SAS)-function models, Hydrology and Earth System Sciences, 27, 3083-3114, https://doi.org/10.5194/hess-27-3083-2023, 2023.

Yang, Y., Zhu, Q., Peng, C., Wang, H., Xue, W., Lin, G., Wen, Z., Chang, J., Wang, M., and Liu, G.: A novel approach for modelling vegetation distributions and analysing vegetation sensitivity through trait-climate relationships in China, Scientific Reports, 6, 24110, https://doi.org/10.1038/srep24110, 2016b.

Zhang, L., Dawes, W., and Walker, G.: Response of mean annual evapotranspiration to vegetation changes at catchment scale, Water resources research, 37, 701-708, https://doi.org/10.1029/2000WR900325, 2001.

Zhang, L., Hickel, K., Dawes, W. R., Chiew, F. H., Western, A. W., and Briggs, P. R.: A rational function approach for estimating mean annual evapotranspiration, Water resources research, 40(2), https://doi.org/10.1029/2003WR002710, 2004.

Zhou, S., Yu, B., Huang, Y., and Wang, G.: The complementary relationship and generation of the Budyko functions, Geophysical Research Letters, 42(6), 1781-1790, https://doi.org/10.1002/2015GL063511, 2015.

810

Table1. Characteristics of the Neckar catchment in Germany

Characteristics	
latitude (N)	48°02′00″-48°46′59″
longitude (E)	8°18′45″-9°56′33″
Area (km^2)	3968
Average annual precipitation (mm yr^{-1})	880
Average annual temperature (°C)	8.39
Elevation range (m)	250-1019
Mean elevation (m)	554
Slope range (°)	0-53
Mean slope (°)	5.80
Forest dominated land (%)	39.6
Grass dominated land (%)	49.6
Wetland (%)	10.8

Table2. Mean annual precipitation P, potential evaporation E_P, temperature T_m, aridity index I_A, evaporative index I_E, parameter ω for parametric Budyko framework, root zone storage capacity $S_{umax,WB}$ and $S_{umax,cal}$ based on respectively water balance data and hydrological model calibration for scenario 1 (entire time period T: 1953-2022) and scenario 2 (four sub- periods t1:1953-1972, t2:1973-1992, t3:1993-2012, and t4:2013-2022).

	Scenario 1	Scenario 2			
	T (1953-2022)	t1 (1953-1972)	t2 (1973-1992)	t3 (1993-2012)	t4 (2013-2022)
P (mm yr^{-1})	876	870	907	915	811
E_P (mm yr^{-1})	867	836	840	884	906
T_M (°C)	8.4	7.4	7.9	8.7	9.5
I_A(-)	0.97	0.96	0.93	0.97	1.12
I_E (-)	0.57	0.58	0.56	0.56	0.59
ω (-)	1.95	2.01	1.98	1.93	1.89
$S_{umax,WB}$ (mm)	105	95	115	95	100
$S_{umax,cal}$ (mm)	116	98	123	99	107

Table 3. Signatures of flow and the associated performance metrics used for model calibration and evaluation. The performance metrics include the Nash–Sutcliffe efficiency (NSE) and the relative error (RE).

Signature	Symbol	Performance metric
Time series of stream flow	Q	NSE_Q
Time series of log(Q)	log(Q)	$NSE_{log(Q)}$
Flow duration curve of log(Q)	$FDC_{log(Q)}$	$NSE_{FDClog(Q)}$
Seasonal runoff coefficient	C_r	NSE_{Cr}
Autocorrelation function of flow (AC)	AC	NSE_{AC}
Runoff coefficient in summer	$C_{r,summer}$	$RE_{Cr,summer}$
Runoff coefficient in winter	$C_{r,winter}$	$RE_{Cr,winter}$

815

820
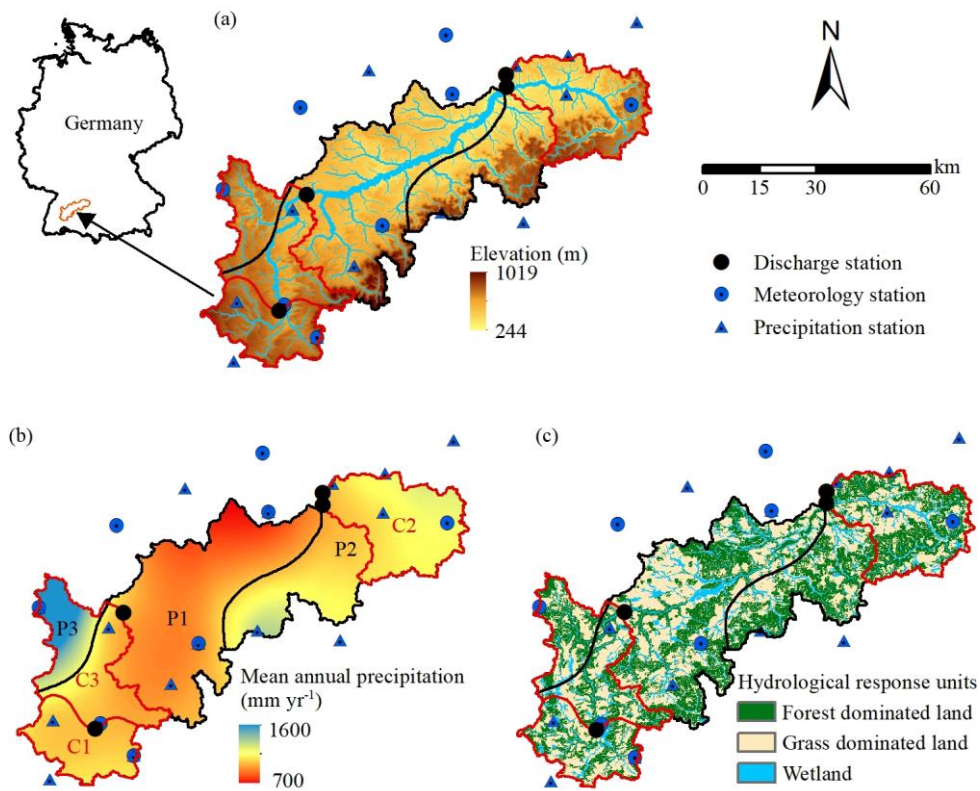
Figure 1. (a) Elevation of the Neckar catchment with discharge and hydro-meteorological stations as well as the water sampling locations used in this study,
(b) the spatial distribution of long-term mean annual precipitation in the upper Neckar catchment and the stratification into three distinct precipitation zones
P1 – P3 (black outline), and the red outlines indicate three sub-catchments (C1:Rottweil, C2: Plochingen at Files river, and C3: Horb) within the upper Neckar
basin, (c) hydrological response units classified according to their land-cover and topographic characteristics.

825
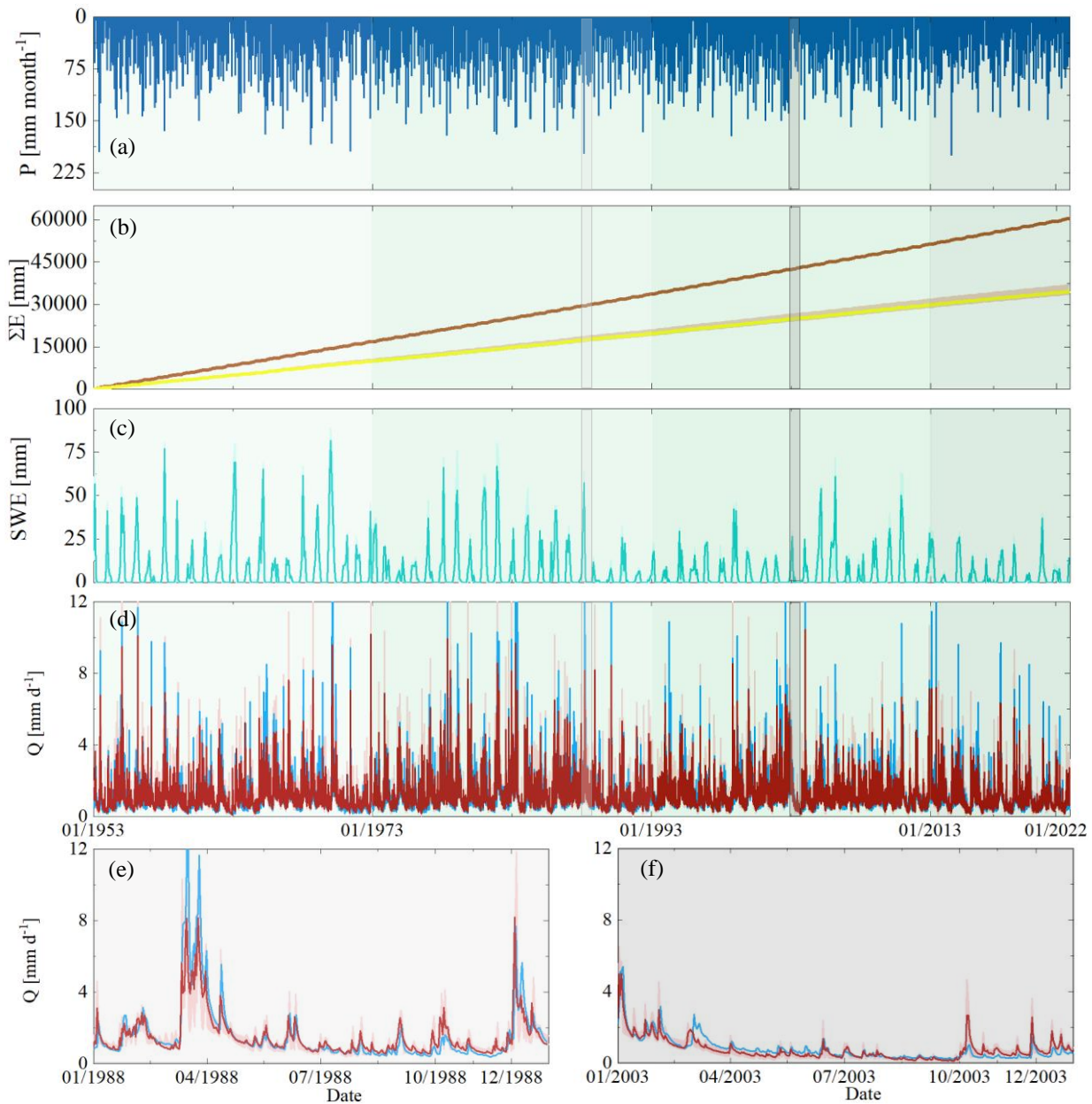
Figure 2. (a) Time series of observed monthly precipitation P; (b) daily cumulative evaporative fluxes for entire time period (1953-2022), where the dark brown line indicates potential evaporation E_P and the yellow lines and the light orange shaded areas show the actual evaporation E_A modelled using the best fit parameter sets and the associated 5th/95th percentiles of all feasible solutions calibrated based on entire time period; (c) monthly maximum values of snow water equivalent (SWE) for 1953-2022 time period where green line indicates the most balanced solution and light green shade indicates the 5th/95th inter-quantile range obtained from all pareto optimal solutions calibrated based on entire time period; (d) observed (blue line) and modelled daily streamflow Q; red line indicates the most balanced solution and the shaded area indicates the 5th/95th percentile of all feasible solutions calibrated based on entire time period, respectively; the different green background shades from lighter to darker indicate sub-time periods from t_1 to t_4; (e) and (f) zoom-in to the observed and modelled streamflow for the selected wet year(light gray shade, 01/01/1988 – 31/12/1988) and dry year (gray shade, 01/01/2003 – 31/12/2003) respectively.
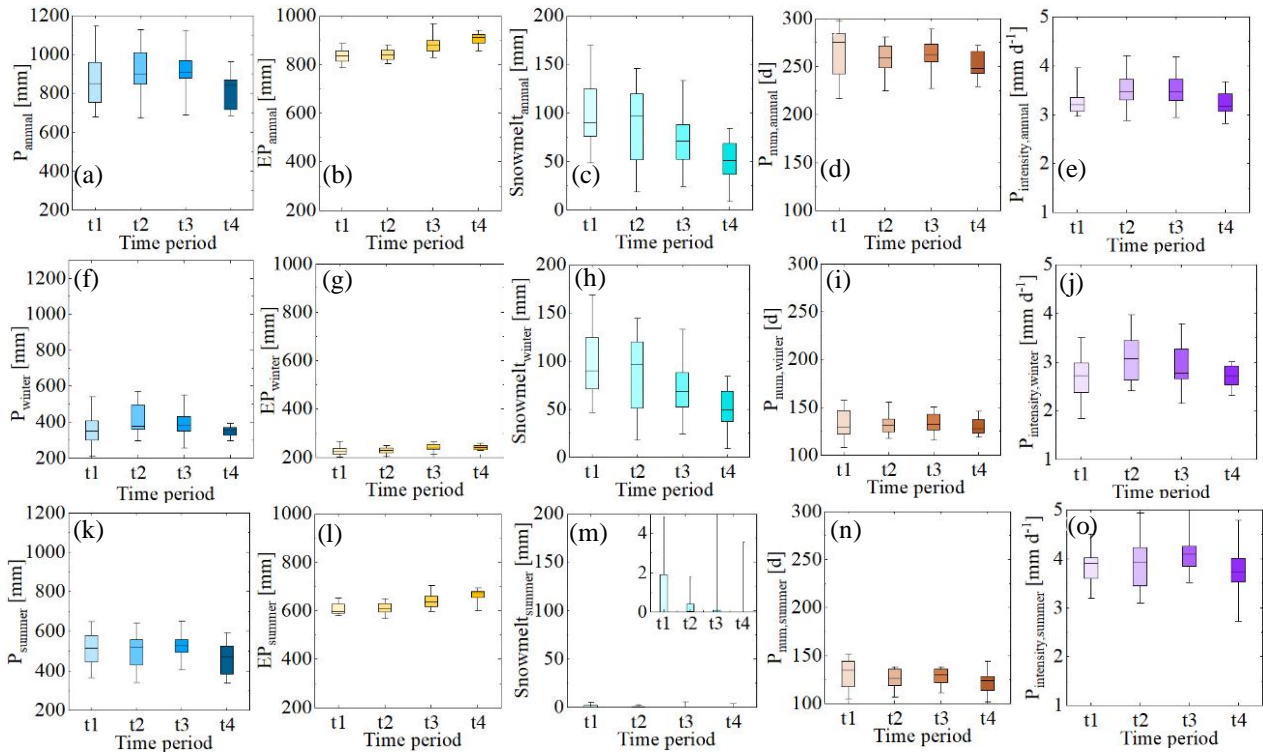
Figure 3. The annual and seasonal variability (i.e., winter and summer) of selected climatic indices including annual averages of precipitation (P), potential evaporation (E_P), estimated snow melt water, the number of precipitation days (P_{num}) and precipitation intensity ($P_{intensity}$) for four sub-time periods (t_1:1953-1972, t_2:1973-1992, t_3:1993-2012, and t_4:2013-2022). (a) – (e) the annual variability of selected climatic indices; (f) – (j) the seasonal variability of selected climatic indices in winter periods; (k) – (o) the seasonal variability of selected climatic indices in summer periods.
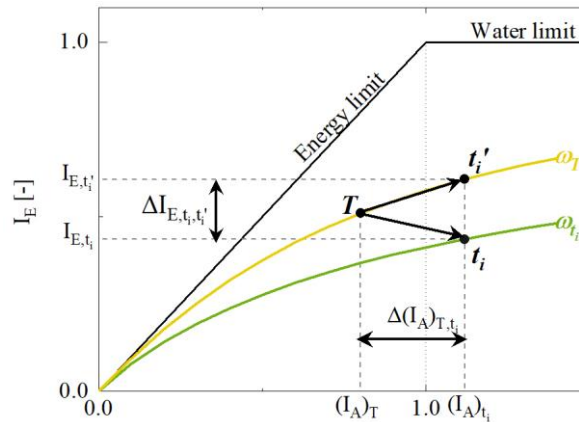
Figure 4. Representation of the Budyko space, which shows the evaporative index ($I_E = 1-Q/P$) as a function of the aridity index ($I_A = E_P/P$) and the water and energy limit. A catchment with the long term mean aridity index $I_{A,T} = E_{P,T}/P_T$ and evaporative index $I_{E,T} = 1-Q_T/P_T$, which is derived from observed entire-time-period data, plots at location T on the parametric Budyko curve with ω_T (yellow line) as the baseline. Based on observed sub-time-period data, with the aridity index $I_{A,ti} = E_{P,ti}/P_{ti}$ and evaporative index $I_{E,ti} = 1-Q_{ti}/P_{ti}$, the same catchment plots at location t_i on the parametric Budyko curve with ω_{ti} (green line). A movement in the Budyko space towards t_i 'along the ω_T curve is shown as a result of a change in the aridity index $I_{A,ti}$ with the assumption that the long-term mean Budyko curve trajectory and the parameter ω is transferable across time for an individual catchment, which results in a significant deviation $\Delta I_{E,ti,ti'}$ between the observed evaporative index $I_{E,ti}$ and the predicted evaporative index $I_{E,ti'}$.

855
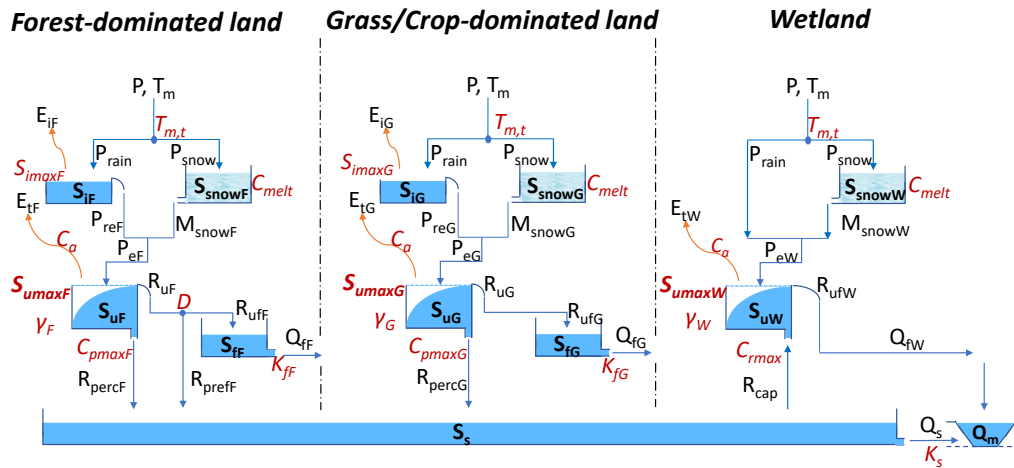
Figure 5. Model structure of the distributed conceptual hydrological model, discretized into three parallel hydrological response units HRU, i.e. forest, grassland and wetland in each precipitation zone P1 – P3. The light blue boxes indicate the hydrologically active individual storage volumes. The arrow lines indicate water fluxes and model parameters are shown in red. All symbols are described in Table S1 in the Supplementary Material.

860
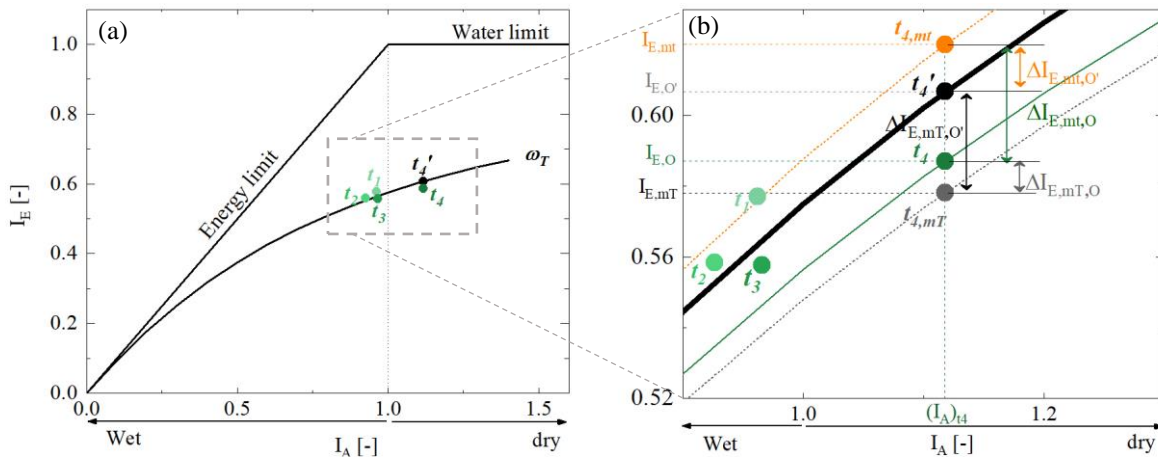
Figure 6. (a) Green dots from light "•" to dark "•" indicate the observed positions for four sub-time periods from t_1 to t_4. The black dot "•" t_4' indicates the expected location on the parametric Budyko curve with ω_T derived from observed entire time period. We select time period t_4 as an example to present the modelled positions in the zoom-in plot (b). The gray dot "•" $t_{4,mT}$ indicates the modelled position based on scenario1 which is with $S_{umax,WB,T}$, and the orange

865 dot "•" $t_{4,mt}$ indicates the modelled position based on scenario 2 which is with $S_{umax,WB,t4}$. $\Delta I_{E,mT,O'}$ (black arrow) indicates the deviation between modelled $I_{E,mT}$ ("•") based on scenario 1 and expected $I_{E,O'}$ ("•"). $\Delta I_{E,mt,O'}$ (orange arrow) indicates the deviation between modelled $I_{E,mt}$ ("•") based on scenario 2 and expected $I_{E,O'}$ ("•"). $\Delta I_{E,mT,O}$ (gray arrow) indicates the deviation between modelled $I_{E,mt}$ ("•") based on scenario 1 and observed $I_{E,O}$ ("•"). $\Delta I_{E,mt,O}$ (green arrow) indicates the deviation between modelled $I_{E,mt}$ ("•") based on scenario 2 and observed $I_{E,O}$ ("•").

870
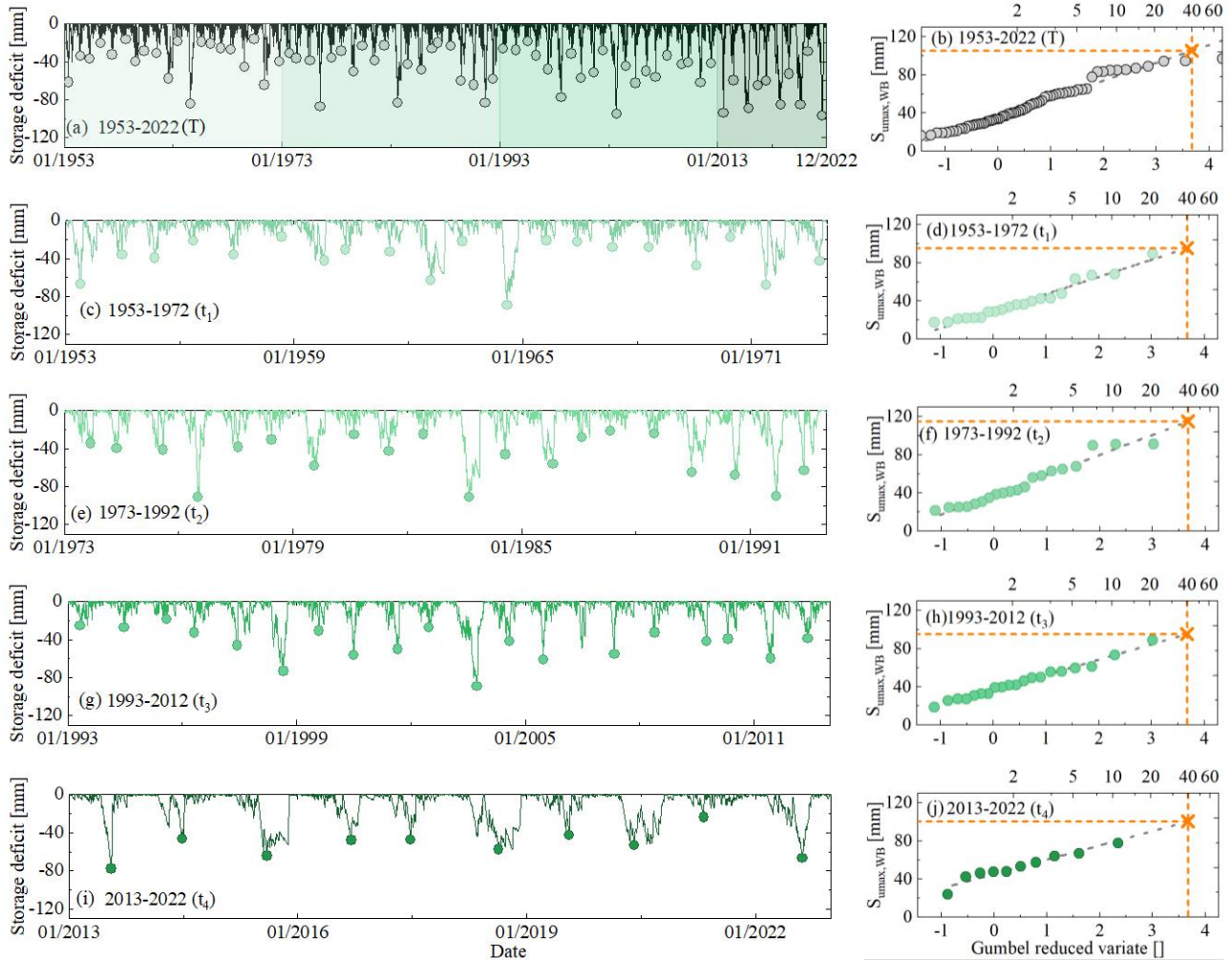
Figure 7. (a), (c), (e), (g) and (i) The time series of storage deficits as calculated by Eq. 7, for entire time period T (1953-2022) and four sub-time periods (green shades from light to dark for time period from t_1 to t_4). The maximum annual deficits are indicated by the dots. (b), (d), (f), (h) and (j) Estimation of S_{umax} as the storage deficit associated with a 40-year return period using the Gumble extreme value distribution for different time periods. The orange crosses indicate the values of S_{umax} for different time periods.

875
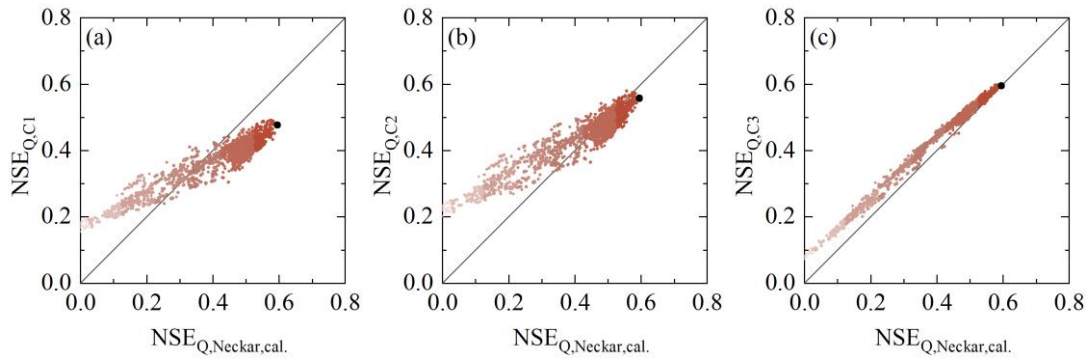
Figure 8. Selected model performance metrics in the entire time period 01/01/1953 – 31/12/2022 of the upper Neckar basins against the model performance in uncalibrated sub-catchment C1: Rottweil, C2: Plochingen at files river, and C3: Horb based parameter sets derived from the calibration for entire time period. The dots indicate all pareto optimal solutions in the multi-objective model performance space. The shades from dark to light indicate the overall model performance based on the Euclidean Distance D_E, with the black solutions representing the overall better solutions (i.e. larger D_E)
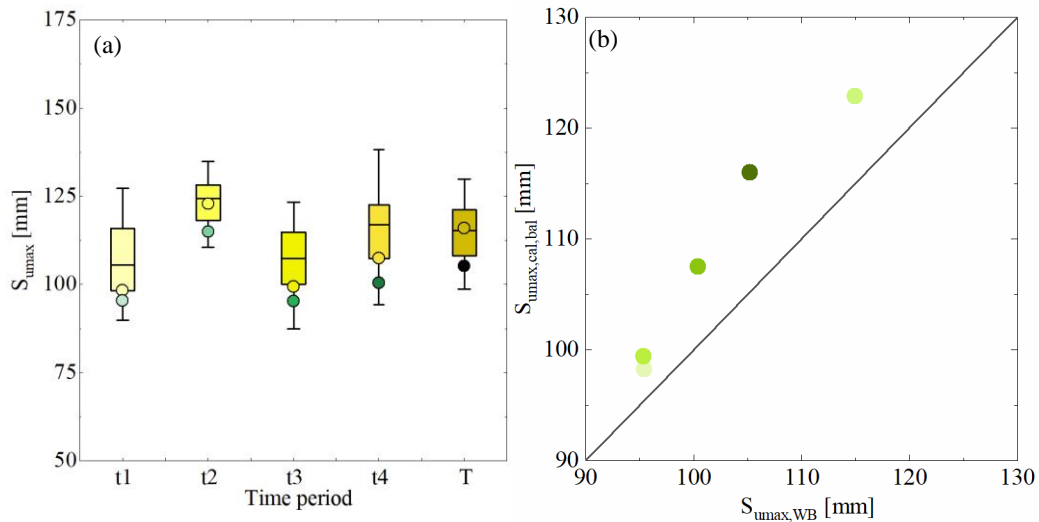
Figure 9. (a) S_{umax} values derived from water-balance method and hydrological model for different time periods. The yellow boxes from light to dark indicate the range of $S_{umax,cal}$ for the sub-time period from t_1 to t_4 and entire time period T based on the corresponding parameter sets derived from the model, yellow dots indicate the corresponding $S_{umax,cal,bal}$ based on the most balanced solution, and green dots indicate the corresponding $S_{umax,WB}$ derived from water-balance method. (b) the values of $S_{umax,cal,bal}$ against $S_{umax,WB}$. The yellow-green dots from light to dark indicate the values of S_{umax} for the sub-time period from t_1 to t_4 and entire time period T.
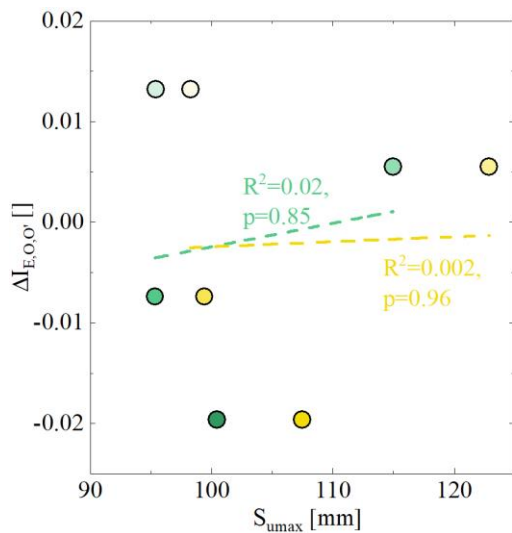
Figure 10. Relationships between the deviations $\Delta I_{E,O,O'}$ and the values of $S_{umax,WB}$ and $S_{umax,cal}$ for four sub-time periods (t_1-t_4) which are respectively derived from the water-balance-method (green circles) and hydrological model calibration (yellow circles).
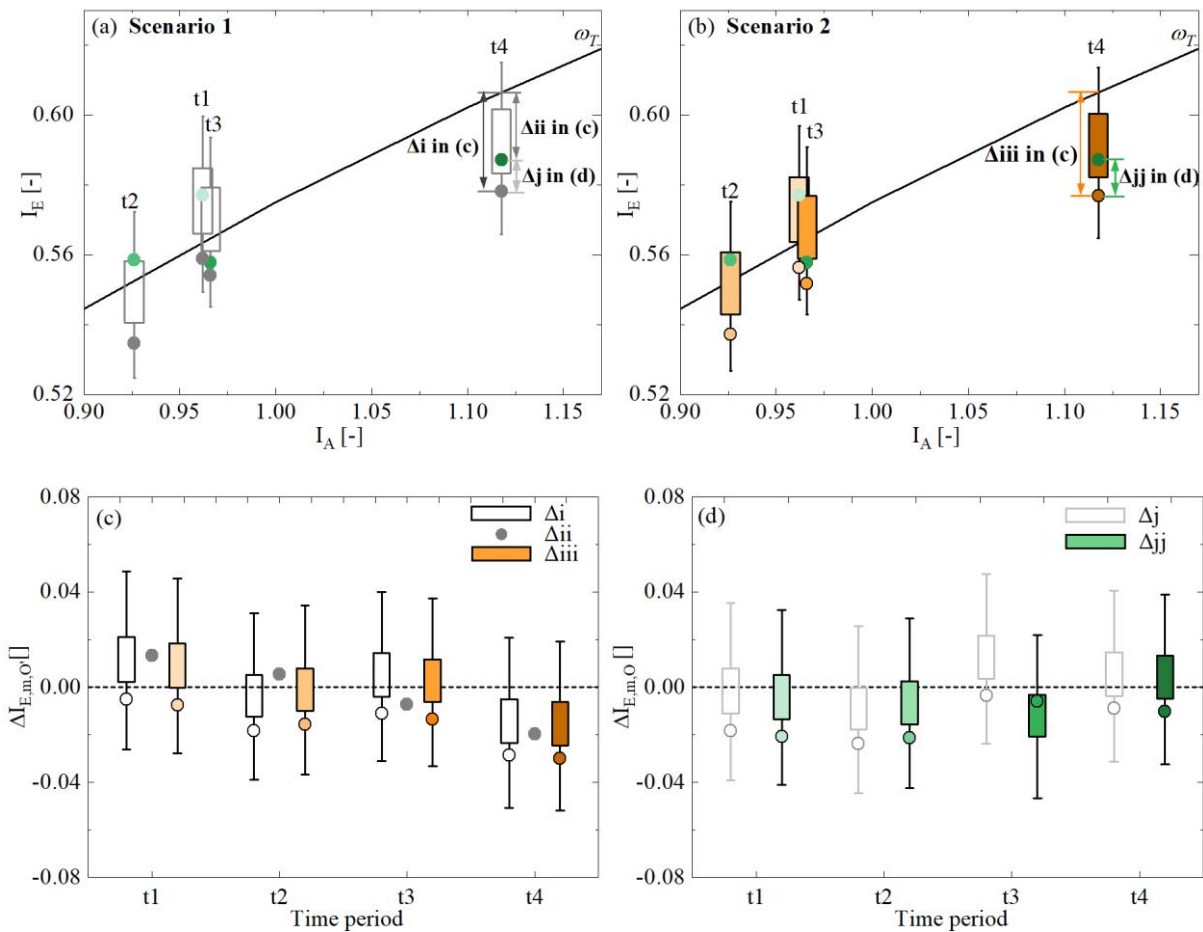
Figure 11. (a) The gray boxes ($I_{E,mT}$) indicate the modelled evaporative index based on all pareto front solutions for four sub-time periods based on scenario 1 with a stationary $S_{umax,WB,T}$ and gray dots based on the most balanced solution based on scenario 1. The green circles from light to dark in (a) and (b) indicate the observed evaporative index for four sub-time periods from t_1 to t_4. (b) The orange circles ($I_{E,mt}$) indicate the modelled evaporative index based on all pareto front solutions for four sub-time periods (from lighter to darker shades) based on scenario 2 with time-variant S_{umax,WB,t_i} and the orange circles based on the most balanced solution for scenario 2. Black boxes in (c) indicate the deviations $\Delta I_{E,mT,O'} = I_{E,mT}-I_{E,O'}$ (Δi)based on all pareto front solutions for four sub-time periods, and the dark gray circles based on the most balanced solution based on scenario 1. Orange boxes in (c) indicate the deviations $\Delta I_{E,mt,O'} = I_{E,mt} -I_{E,O'}$ (Δiii) based on all pareto front solutions for four sub-time periods, and the orange circles based on the most balanced solution for scenario 2. The gray dots indicate the deviation $\Delta I_{E,O,O'}$ (Δii) between observed $I_{E,O}$ for each sub-time period and corresponding expected $I_{E,O'}$. Light gray boxes in (d) indicate the deviations $\Delta I_{E,mT,O} = I_{E,mT}-I_{E,O}$ (Δj) based on all pareto front solutions for four sub-time periods, and the gray circles based on the most balanced solution. Green boxes in (d) indicate the deviations $\Delta I_{E,mt,O} = I_{E,mt} -I_{E,O}$ (Δjj) based on all pareto front solutions for four sub-time periods, and the green circles based on the most balanced solution.
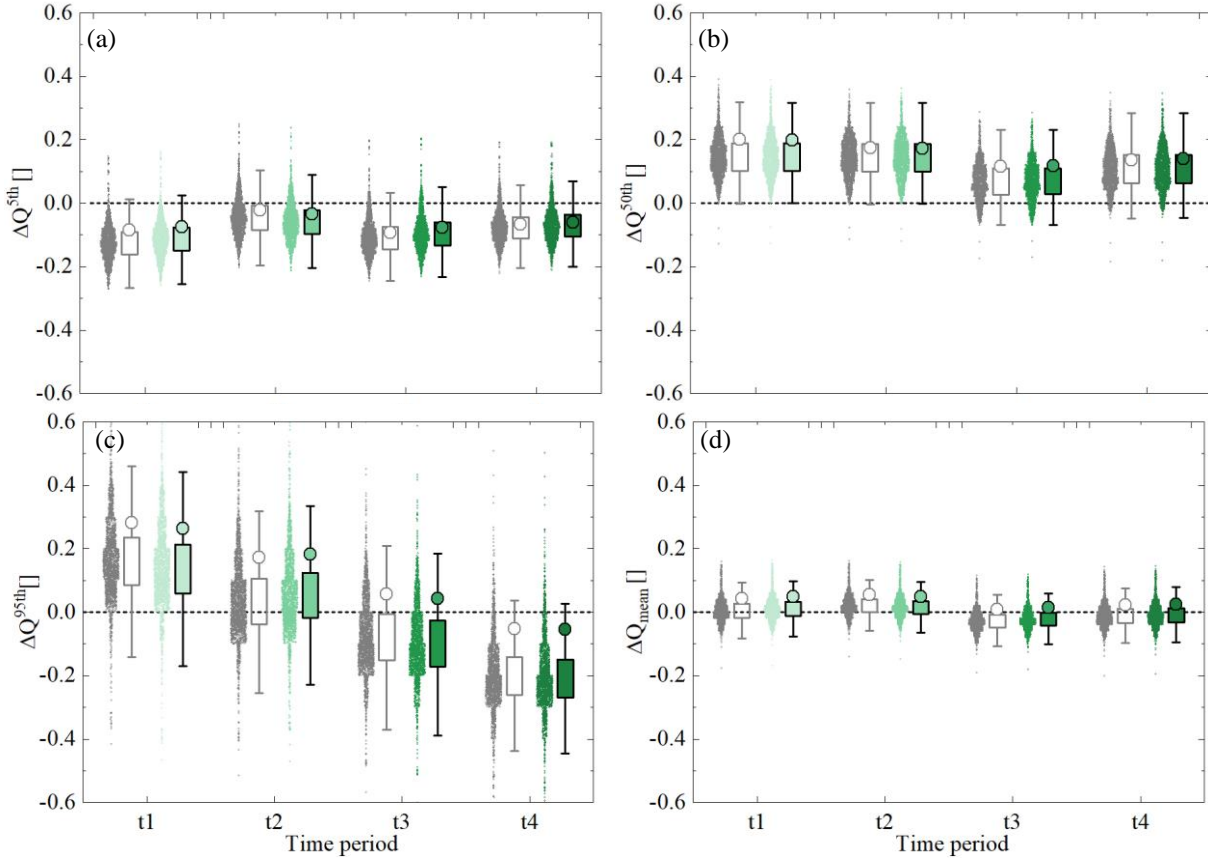
Figure 12. The relative errors of observed and modelled high (Q^{5th}), median (Q^{50th}), and low (Q^{95th}) flow quantiles and the mean Q for different time periods based on two scenarios. The gray shades and corresponding dots indicate the relative errors based on scenario 1 with all pareto front solutions and the gray circles indicate the most balanced solution. The corresponding values for scenario 2 are shown in green.
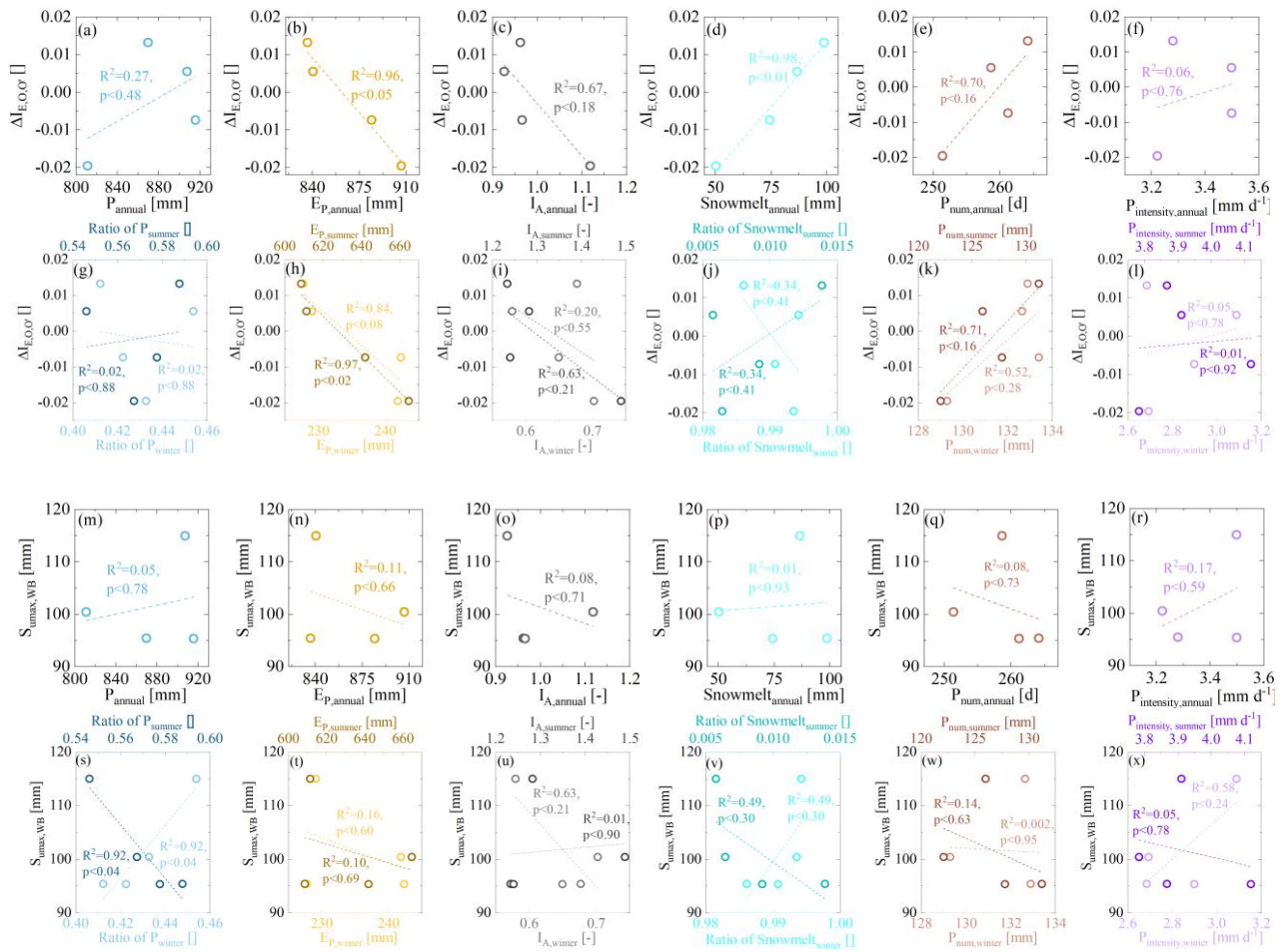
Figure 13. Relationships between the temporal fluctuation of the deviations ($\Delta I_{E,O,O'}$, the black dots in Fig. 10a), and $S_{umax,WB}$ and climate indices including precipitation (P), potential evaporation (E_P), aridity index (I_A), estimated snow melt water (Snowmelt), the number of precipitation days (P_{num}) and precipitation intensity ($P_{intensity}$) for the four sub-time periods. Relationships between the temporal fluctuation of the deviations ($\Delta I_{E,O,O'}$, the black dots in Fig. 10a) and climate indices for the four sub-time periods are shown in the first two rows (a)-(l) (i.e., (a)-(f) $\Delta I_{E,O,O'}$ vs. annual climatic indices, (g)-(l) $\Delta I_{E,O,O'}$ vs. seasonal climatic indices). Relationships between the temporal fluctuation of $S_{umax,WB}$ derived from the water-balance-method and climate indices for the four sub-time periods are shown in the last two rows (m)-(x) (i.e., (m)-(r) $S_{umax,WB}$ vs. annual climatic indices, (s)-(x) $S_{umax,WB}$ vs. seasonal climatic indices).